

Response to the comments of Anonymous Referee #1

Referee General Comment:

This manuscript explores the equilibrium timescale and mixing timescale of IVOC and LVOC with particles considering different phase states. The work combines the authors' previous KM-GAP model (Shiraiwa et al., 2012) with the authors' recent glass transition model (Shiraiwa et al., 2017; DeRieux et al. 2018) to understand the interplay among equilibrium timescale, temperature, relative humidity, and the glass transition temperature of the aerosols.

Besides the numerical results obtained from the model shown in Figure 1-5, the manuscript provides two more useful results: (1) when there is no diffusion limitation within the particle, the gases that have higher saturation mass concentrations will reach gas-particle equilibrium faster; (2) when there is strong diffusion limitation within the particle, gases that have lower volatility may reach gas-particle equilibrium (locally) faster than VOCs with higher volatility. One of the implications is that at a lower temperature (upper troposphere) or when dealing with highly viscous particles, the particle growth process may need to be treated kinetically.

The authors used a numerical model to obtain result #1 above, and it agrees with the findings in Liu et al. 2012 in which an analytical model was used. It is nice to see two different approaches come with the same results and can validate each other. On the other hand, result #2 is more interesting because it shows that local equilibrium could be reached relatively faster for low volatility species when the particle phase is highly viscous. The manuscript also illustrates some concepts that can be commonly misused by folks, such as the difference between equilibrium timescale and the mixing timescale. Because some of the results have been previously discussed in or can be easily inferred from other publications (Liu et al. 2012, Shiraiwa et al. 2011&2012), the novelty of the manuscript needs to be improved. I suggest that the author focus on result #2, which is novel, and use it to make further predictions regarding the physical and chemical processes of aerosols.

Response: We thank Anonymous Referee #1 for the review and the positive evaluation of our manuscript. Following your constructive suggestions, in the revised manuscript, we add (1) a contour plot of τ_{eq} as a function of bulk diffusivity and volatility to illustrate under what conditions the fast local equilibrium may be achieved to highlight the result #2 you are interested; and (2) simulations for open systems and the results are compared with τ_{eq} in a closed system. We find partitioning of LVOC is very different in open and closed systems and the corresponding implications in SOA evolution in ambient air and chemical transport models are further broadened. As Referee #2 pointed, this publication essentially closes the loop between predicting phase state and calculating the gas/particle equilibration time. We believe after addition of above two aspects, the novelty of the revised manuscript is improved. Please see the detailed response below.

Referee Major Comment:

(1) For instance, what is the relationship between particle sizes and condensation/evaporation kinetics of gases with different volatility interacting with particles with various viscosity?

Response: Thanks for this helpful comment. In our ACPD manuscript, Figure 5 (Figure 6b and d in the revised manuscript) has shown the relationship between τ_{eq} and particle size for LVOC condensing on less viscous as well as highly viscous particles. In the revised manuscript, we add comparable calculation for SVOC (Fig. 6a, c). This issue has also been discussed in previous studies, e.g., Liu et al. (2013) and Mai et al. (2015). For example, Mai et al. (2015) presented τ_{eq} as a function of particle diameter and volatility, showing that τ_{eq} increases as the particle diameter increases or the volatility of the condensing species decreases when particles are liquid with partitioning limited by interfacial transport. When particles are highly viscous with bulk diffusion-limited partitioning, the time to reach full equilibrium depends on mixing timescale. The following discussions have been added in the revised manuscript:

Lines 259-263: “Previous studies have shown that τ_{eq} depends on particle size (Liu et al., 2013; Zaveri et al., 2014; Mai et al., 2015) and particle mass loadings (Shiraiwa and Seinfeld, 2012; Saleh et al., 2013). For further examination of these effects at different T , Figure 6 shows the dependence of τ_{eq} of SVOC ($C^0 = 10 \mu\text{g m}^{-3}$) and LVOC ($C^0 = 0.1 \mu\text{g m}^{-3}$) on the mass concentration and the diameter of pre-existing particles”.

Lines 271-274: “When particles are less viscous at 298 K ($D_b = 10^{-11} \text{ cm}^2 \text{ s}^{-1}$) τ_{eq} of SVOC is shorter than that of LVOC for the same particle size and mass loadings. When partitioning into highly viscous particles at 250 K ($D_b = 10^{-18} \text{ cm}^2 \text{ s}^{-1}$), SVOC takes longer time than LVOC to reach equilibrium”.

Lines 275-285: “Typical ambient organic mass concentrations in Beijing, Centreville in southeastern US, Amazon Basin, and Hyytiälä, Finland are indicated in Fig. 6. The particle phase state was observed to be mostly liquid in highly polluted episodes in Beijing (Liu et al., 2017), under typical atmospheric conditions in the southeastern US (Pajunoja et al., 2016), and under background conditions in Amazonia (Bateman et al., 2017). At these conditions τ_{eq} should be mostly less than 30 minutes (Fig. 6a, b). Particles were measured to be semi-solid or amorphous solid in clear days in Beijing (Liu et al., 2017), in Amazonia when influenced by anthropogenic emissions (Bateman et al., 2017), and the boreal forest in Finland (Virtanen et al., 2010). Under these conditions and also when particles are transported to the free troposphere, τ_{eq} can be longer than 1 hour especially in remote areas with low mass loadings (Fig. 6c, d)”.

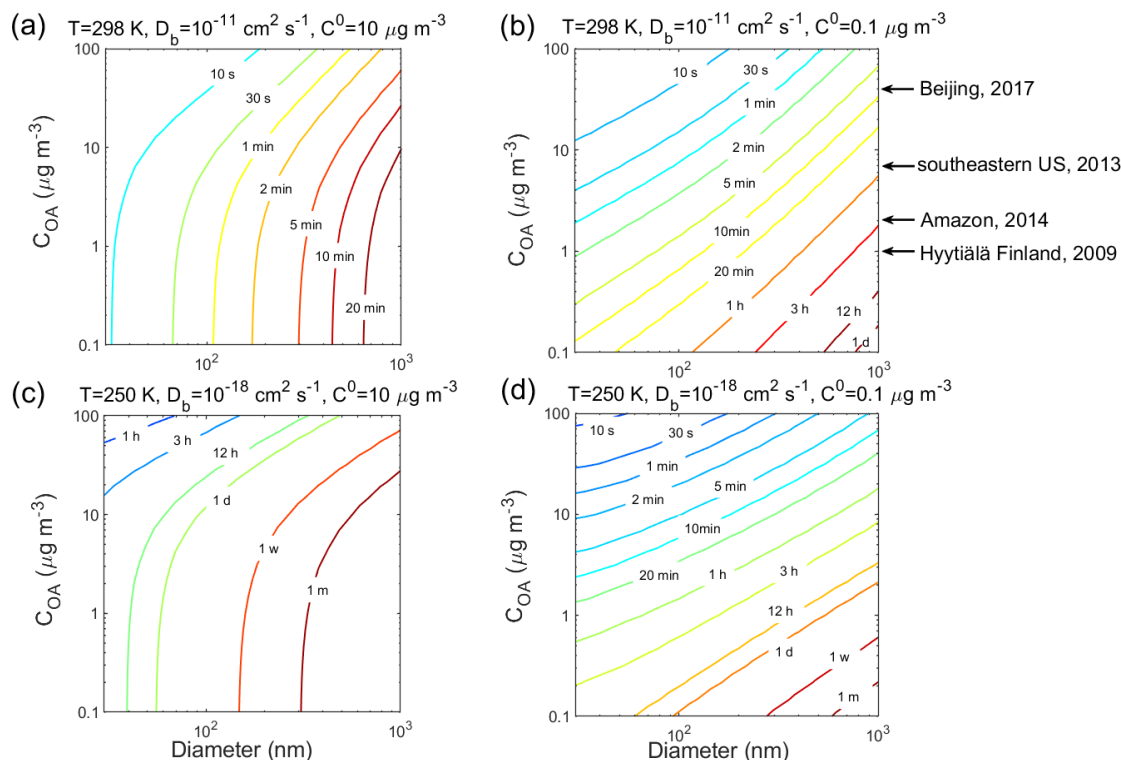


Figure 6. Equilibration timescale (τ_{eq}) for (a, c) SVOC ($C^0 = 10 \mu\text{g m}^{-3}$) and (b, d) LVOC ($C^0 = 0.1 \mu\text{g m}^{-3}$) as a function of particle diameter (nm) and mass concentration ($\mu\text{g m}^{-3}$) of pre-existing particles at 60% RH and T of (a-b) 298 K and (c-d) 250 K in the closed system. The glass transition temperature of pre-existing particles under dry conditions ($T_{g,org}$) is set to be 270 K, which leads to D_b of (a-b) $10^{-11} \text{ cm}^2 \text{ s}^{-1}$ and (c-d) $10^{-18} \text{ cm}^2 \text{ s}^{-1}$. Ambient organic mass concentrations are indicated with arrows.

(2) I would also be curious to know what is the boundary criteria for result #2 to happen, i.e., how viscous would the particles have to be or how low the volatility of the VOC have to be in order to reach relatively fast local equilibrium? The author can also explore the effects of equilibrium partitioning when the gases can both partition in and react with the particle phase.

Response: This is a very interesting point. To address your question, we conducted additional simulations for τ_{eq} as a function of bulk diffusivity and volatility for both open and closed systems. The results of such simulations are shown in new Figure 4. The effect of particle-phase reactions on SOA partitioning is an important question, which is beyond the scope of this study. We plan to follow up on this issue in our future study. The following discussions have been added in the revised manuscript:

Lines 194-201: “We further computed τ_{eq} as a function of D_b and C^0 in the closed system. As shown in Fig. 4a, when D_b is higher than $\sim 10^{-13} \text{ cm}^2 \text{ s}^{-1}$, τ_{eq} is insensitive to bulk diffusivity but sensitive to volatility: decreasing volatility increases τ_{eq} in this regime. In the regime with D_b lower than $\sim 10^{-13} \text{ cm}^2 \text{ s}^{-1}$ and C^0 higher than $\sim 10 \mu\text{g m}^{-3}$, τ_{eq} is controlled by bulk diffusivity: τ_{eq} increases from 30 s to longer than 1 year as D_b decreases from $10^{-13} \text{ cm}^2 \text{ s}^{-1}$ to $10^{-20} \text{ cm}^2 \text{ s}^{-1}$. In the regime with $D_b < \sim 10^{-13} \text{ cm}^2 \text{ s}^{-1}$

and $C^0 < \sim 10 \mu\text{g m}^{-3}$, τ_{eq} depends on both diffusivity and volatility. Decreasing volatility would lead to shorter τ_{eq} due to an establishment of local equilibrium of LVOC”.

Lines 221-225: “Figure 4b shows simulated evaporation timescales as a function of D_b and C^0 in an open system, which agrees very well with Fig. 3 in Liu et al. (2016). It shows that for less viscous particles τ_{eq} is limited by volatility, while for highly viscous particles τ_{eq} is insensitive to volatility and controlled by bulk diffusivity”.

Lines 127-128: “Particle-phase reactions and their potential impacts on particle viscosity are also not considered in this study”.

Lines 361-369: “Incorporation of the particle-phase formation of oligomers and other multifunctional high molar mass compounds can lead to a reduced bulk diffusivity (Pfrang et al., 2011; Hosny et al., 2016), which may prolong the equilibration timescales. Decomposition of highly oxidized molecules (e.g., organic hydroperoxides) in water may also affect gas-particle partitioning (Tong et al., 2016). Current simulations are focused on trace amount of SVOC or LVOC condensing on mono-dispersed particles with negligible particle growth. Potential phase transition in the course of particle growth/evaporation should also be incorporated in future simulations”.

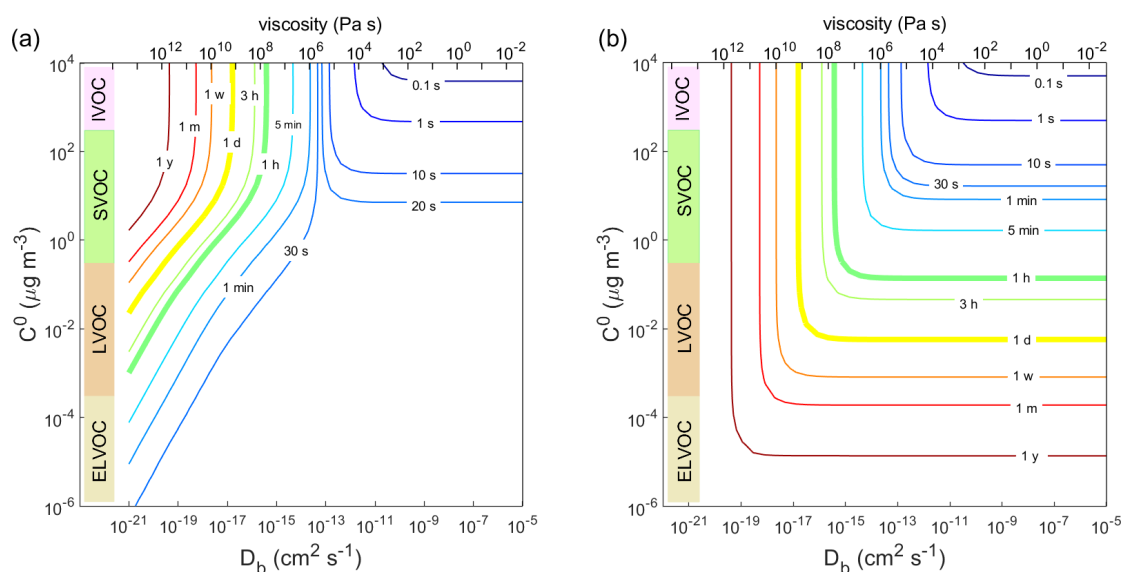


Figure 4. Contour plot of equilibration timescale (τ_{eq}) as a function of bulk diffusivity (D_b) and saturation mass concentration (C^0) for (a) condensation in the closed system and (b) evaporation in the open system. The initial mass concentration of pre-existing particles is set to be $20 \mu\text{g m}^{-3}$ with the number concentrations of $3 \times 10^4 \text{ cm}^{-3}$ and the initial particle diameter of 100 nm. Viscosity is calculated from the Stokes-Einstein equation assuming the effective molecular radius of 10^{-8} cm at T of 298 K.

(3) My other question is that most of the modeling results shown the manuscript assumed that the gas-particle is in a closed system. How realistic is the closed system in ambient environment? Would the ambient environment often be an open system for

evaporation kinetics?

Response: Thanks for this helpful comment. To address this question, we add simulations for an open system (Fig. 4b, S5, and S7) in the revised manuscript. The following discussions have been added in the revised manuscript.

Lines 202-208: “In an open system with fixed vapor concentration (Fig. S5), τ_{eq} of SVOC is slightly longer but on the same order of magnitude as τ_{eq} in the closed system, as relatively small amounts of SVOC need to condense to reach equilibrium. In contrast, τ_{eq} of LVOC in the open system become dramatically longer as LVOC continue to condense into the particle phase because of low volatility (Pankow, 1994). For further simulations we focus mainly on the closed system and the corresponding simulations for the open system are provided in the supplement”.

Lines 221-225: “Figure 4b shows simulated evaporation timescales as a function of D_b and C^0 in an open system, which agrees very well with Fig. 3 in Liu et al. (2016). It shows that for less viscous particles τ_{eq} is limited by volatility, while for highly viscous particles τ_{eq} is insensitive to volatility and controlled by bulk diffusivity”.

Lines 242-244: “The corresponding simulations of SVOC partitioning in the open system (Fig. S7) show a similar pattern as τ_{eq} in the closed system”.

Lines 306-312: “The timescale of gas-particle partitioning can be different in closed or open systems especially for LVOC (Fig. 4, S7). The closed system simulations represent SOA partitioning in chamber experiments and in closed atmospheric air mass, which could be justified well within seconds-to-minutes timescales and possibly up to hours depending on meteorological conditions. The real atmosphere may be approximated better as an open system due to dilution and chemical production and loss especially at longer timescales”.

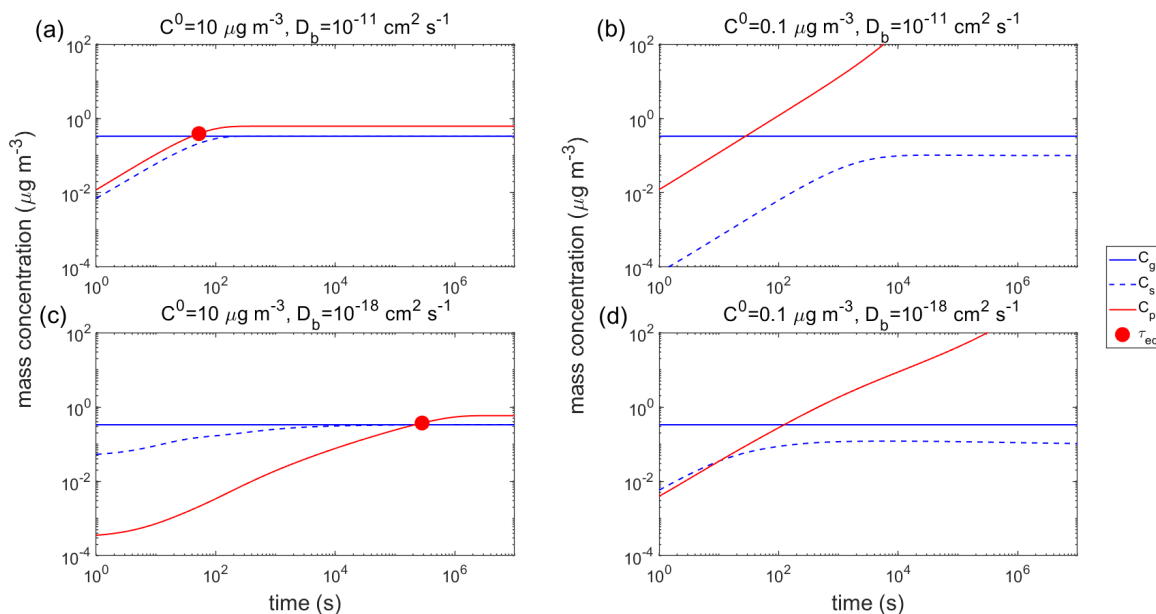


Figure S5. Temporal evolution of mass concentrations of the condensing compound Z in the gas phase (C_g), just above the particle surface (C_s), and in the particle phase (C_p) in the open system. τ_{eq} is marked with the red circle. RH = 60% and T is (a–b) 298 K and (c–d) 250 K. The C^0 of Z is (a, c) $10 \mu\text{g m}^{-3}$ and (b, d) $0.1 \mu\text{g m}^{-3}$. The

glass transition temperature of pre-existing particles under dry conditions ($T_{g,org}$) is set to be 270 K, which leads to D_b of (a–b) $10^{-11} \text{ cm}^2 \text{ s}^{-1}$ and (c–d) $10^{-18} \text{ cm}^2 \text{ s}^{-1}$. The initial mass concentration of pre-existing particles is set to be $20 \mu\text{g m}^{-3}$ with the number concentrations of $3 \times 10^4 \text{ cm}^{-3}$ and the initial particle diameter of 100 nm.

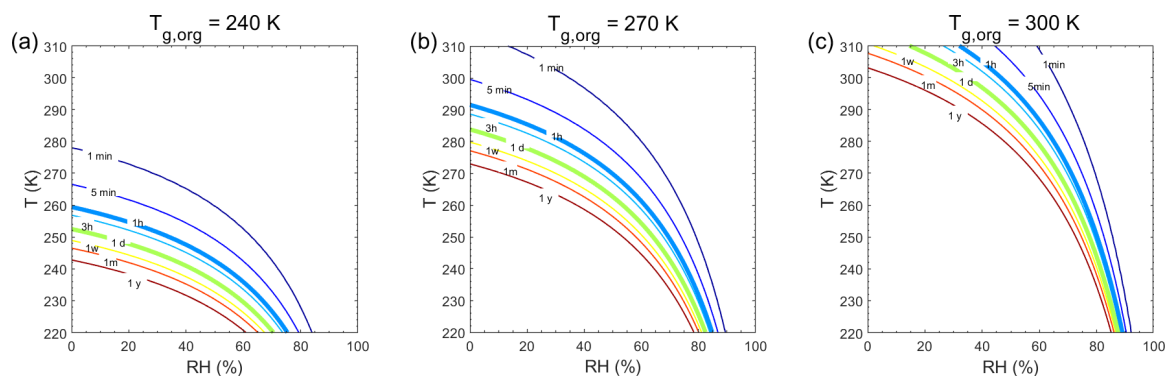


Figure S7. Equilibration timescale (τ_{eq}) as a function of temperature and relative humidity in the open system. The glass transition temperatures of pre-existing particles at dry conditions ($T_{g,org}$) are (a) 240 K, (b) 270 K, and (c) 300 K, respectively. The saturation mass concentration (C^0) of the condensing compound is $10 \mu\text{g m}^{-3}$ (SVOC). The mass concentration of pre-existing particles is set to be $20 \mu\text{g m}^{-3}$ with the number concentrations of $3 \times 10^4 \text{ cm}^{-3}$ and the initial particle diameter of 100 nm.

Referee Minor Comments:

The author should also include Price et al. 2015 in the reference list in line 115.

Reference: Shiraiwa et al. 2011: doi.org/10.1073/pnas.1103045108

Liu et al. 2012: doi.org/10.1080/02786826.2012.730163

Shiraiwa et al. 2012: doi.org/10.1029/2012GL054008

Price et al. 2015: doi.org/10.1039/C5SC00685F

Response: Price et al. (2015) has been included on Line 123 in the revised manuscript.

Besides this, Liu et al. (2013) has been included on Lines 181, 259 and 357.

Liu, C., Shi, S., Weschler, C., Zhao, B. and Zhang, Y.: Analysis of the dynamic interaction between SVOCs and airborne particles, *Aerosol Sci. Technol.*, 47, 125-136, <https://doi.org/10.1080/02786826.2012.730163>, 2013.

Response to the comments of Anonymous Referee #2

Referee General Comment:

In this manuscript, the authors use simulations to calculate the gas/particle equilibration time for secondary organic aerosol as a function of temperature, relative humidity, and SOA microphysical properties. The topic of SOA partitioning, equilibration, and phase state are highly relevant in atmospheric chemistry, the topic is timely, and will be of interest to the readers of ACP. This work is a logical extension of the previous work done by the PI. It essentially combines work in predicting the phase state of particles as a function of atmospheric conditions with work on calculating gas/particle equilibration times (Shiraiwa et al., 2017; Shiraiwa and Seinfeld, 2012). Based on past results from the PI on these topics, the present results are not particularly surprising, but I think there is enough new material here to warrant publication. This publication essentially closes the loop between predicting phase state and calculating the gas/particle equilibration time. With that said, there are a few areas that could be improved before publication. The authors could do a better job of calling out, in the manuscript, what is new unique about this manuscript relative to the previous publications by the PI. A few of the conclusions reached in this work also seem to contradict the PI's previous publications and the authors should clear this up. The authors could help readers put this work into context if they explain why they make certain assumptions in their model (i.e., a closed system), offer some insights into how realistic these assumptions are relative to the ambient atmosphere, and explain how their conclusions would be different if/when the assumptions are not atmospherically representative. While the manuscript is generally well written and clear, there was one section that was somewhat confusing and should be clarified before publication. With that said, there are no major shortcomings with the manuscript and, providing the authors make some revisions, I have no reservations about recommending this manuscript for publication in ACP.

Responses: We thank Anonymous Referee #2 for the review and the positive evaluation of our manuscript. As you pointed out, this is the first study to directly relate equilibration timescale of SOA partitioning to ambient temperature and relative humidity, which has important implications in treatment of SOA evolution in chemical transport models. The novelty of the revised manuscript is further strengthened by two additional new results. Firstly, we add a contour plot of τ_{eq} as a function of bulk diffusivity and volatility to define the regimes of diffusivity-limited and volatility-limited partitioning. Secondly, we add simulations for open systems and the results are compared with τ_{eq} in closed systems. The implications of τ_{eq} in closed and open systems are further broadened for SOA evolution in ambient atmosphere and chemical transport models. Following your suggestion, we clarify that apparently contradicting conclusions regarding τ_{eq} of LVOC actually are consistent with PI's previous publication (e.g., Shiraiwa & Seinfeld, 2012). We also revise the last figure and associated section for better presentation of our results. Please see the detailed response below.

Referee Major Comment:

(1) Lines 23-25, Figure A1, and elsewhere. In the present manuscript the authors conclude that the equilibration timescale for low volatile compounds is shorter than for semi-volatile compounds when other conditions are equal. However, Shiraiwa and Seinfeld 2012 report the opposite (see for example Figure 2), with ELVOC's having longer equilibration times than SVOCs (Shiraiwa and Seinfeld, 2012). The authors should comment in the text on why these studies reach opposite conclusions.

Response: The results in this study are actually consistent with Shiraiwa and Seinfeld (2012) even though our previous statements on Lines 23-25 were somewhat misleading. Figure 2 in Shiraiwa and Seinfeld (2012) was presented for liquid particles showing that τ_{eq} of LVOC is longer, which agreed with the simulations in our current study showing that for less viscous particles LVOC takes longer time than SVOC to reach equilibrium (Fig. 2a-b). Shiraiwa and Seinfeld (2012) did not compare τ_{eq} of LVOC and SVOC condensing on highly viscous particles, which has been simulated in current study showing that τ_{eq} of LVOC is shorter (Fig. 2c-d). We clarified this point on Line 23 in the revised manuscript. In addition, we add Fig. 4 in the revised manuscript to systematically evaluate the dependence of τ_{eq} on both volatility and bulk diffusivity. Please also refer to our response to Comment (2) of Referee #1.

(2) Lines 115-123. I understand that the authors need to make some assumptions or approximations in their model/calculations. I am trying to understand how atmospherically realistic these assumptions are. The two main assumptions in the present model are of a closed system and that the condensation of molecule Z does not alter the composition and microphysical properties of the pre-existing particles. It is clear that the real atmosphere isn't a closed system. The argument could be made that on seconds-to-minutes timescales, it may approximate a closed system, but the processes that authors are modeling are sometimes occurring on timescales of hours or even days. In addition, one of the author's major conclusions is that low volatility material reaches equilibrium more slowly than higher volatility material. I understand why this is the case in a closed system, but would this conclusion also hold in an open system like in the atmosphere with a constant dilution and/or loss of gas-phase molecules? A plume transported from the surface to the upper troposphere would experience an evaporative driving force where this model seems focused on cases where the driving force is toward the particle phase (condensation). With respect to a single compound (Z) changing the composition and microphysical properties, it may be true that a single molecule or even a few molecules rarely make up the bulk of the SOA mass. However, in the real atmosphere, particles obviously grow and their composition and microphysical properties change as SOA condenses. The PI of this manuscript has previously used kinetic modeling to reproduce particle growth, so I'm not really clear on why these assumptions needed to be made (Shiraiwa et al., 2013). In the both cases, I think it is important that the authors explain: why they chose to make these assumptions, how likely it is that these assumptions are representative of the atmosphere, and how their conclusions would likely be different if the assumptions are not correct.

Response: Thanks for this helpful comment. Based on your suggestions we add

simulations for an open system (Fig. 4b, S5 and S7) in the revised manuscript. Figure S5 and S7 show that for condensation of SVOC, τ_{eq} is slightly longer but on the same order of magnitude as τ_{eq} in the closed system. In contrast, τ_{eq} of LVOC condensation in the open system become dramatically longer as LVOC keep condensing into the particle phase because of low volatility. For evaporation in an open system with continuous removal/dilution of gas-phase LVOC, τ_{eq} of LVOC is also much longer than that in a closed system due to continuous evaporation (Fig. 4b). For the details please refer to the response to Comment (3) of Referee #1. The implications of τ_{eq} in closed versus open systems in SOA evolution are broadened. In the revised manuscript we state that:

Lines 306-312: “The timescale of gas-particle partitioning can be different in closed or open systems especially for LVOC (Fig. 4, S7). The closed system simulations represent SOA partitioning in chamber experiments and in closed atmospheric air mass, which could be justified well within seconds-to-minutes timescales and possibly up to hours depending on meteorological conditions. The real atmosphere may be approximated better as an open system due to dilution and chemical production and loss especially at longer timescales”.

We agree that condensation of substantial amounts of materials may lead to changes in particle microphysical properties including phase state and viscosity, which is beyond the scope of current study, even though this is indeed an important aspect. In this study we let only trace amounts to condense so that physical properties including size and phase state would remain unaffected. As KM-GAP can indeed treat evolution of particle properties upon particle growth/evaporation, we plan to explore this aspect systematically by varying particle-phase reaction rates and resulting impacts on phase state in future studies. Following your suggestion, in the revised manuscript we broaden the discussion as below:

Lines 361-369: “Incorporation of the particle-phase formation of oligomers and other multifunctional high molar mass compounds can lead to a reduced bulk diffusivity (Pfrang et al., 2011; Hosny et al., 2016), which may prolong the equilibration timescales. Decomposition of highly oxidized molecules (e.g., organic hydroperoxides) in water may also affect gas-particle partitioning (Tong et al., 2016). Current simulations are focused on trace amount of SVOC or LVOC condensing on mono-dispersed particles with negligible particle growth. Potential phase transition in the course of particle growth/evaporation should also be incorporated in future simulations”.

(3) Lines 276-292 and Figure 5. This figure and associated text was confusing. The figure was confusing because particle diameter and total mass loading are typically not independent of one another in a model or in the atmosphere. I eventually understood the point the authors were trying to make. Perhaps providing some context by pointing out where different atmospheric regimes lie (i.e., remote, typical continental, polluted) in the figure would help. The associated text is also confusing; it wasn't clear what point the authors were trying to make here. They seem to postulate several different processes which could determine particle equilibration

timescales (e.g., bulk diffusion, gas-diffusion). Can't the KM-GAP model be used to clear this up? Overall, I'm not sure what message the authors are trying to convey here.

Response: Following your suggestion, we indicate typical ambient organic mass concentrations in Beijing (Liu et al., 2017), southeastern US (Pajunoja et al., 2016), Amazon Basin (Bateman et al., 2017), and Hyytiälä, Finland (Virtanen et a., 2010) in Fig. 6, where ambient phase state measurements are available. Figure 6 indeed has implications on how different ambient conditions have effect on SOA partitioning. For clarification, the following discussions have been added in the revised manuscript.

Lines 259-261: “Previous studies have shown that τ_{eq} depends on particle size (Liu et al., 2013; Zaveri et al., 2014; Mai et al., 2015) and particle mass loadings (Shiraiwa and Seinfeld, 2012; Saleh et al., 2013). For further examination of these effects at different $T...$ ”.

Lines 275-285: “Typical ambient organic mass concentrations in Beijing, Centreville in southeastern US, Amazon Basin, and Hyytiälä, Finland are indicated in Fig. 6. The particle phase state was observed to be mostly liquid in highly polluted episodes in Beijing (Liu et al., 2017), under typical atmospheric conditions in the southeastern US (Pajunoja et al., 2016), and under background conditions in Amazonia (Bateman et al., 2017). At these conditions τ_{eq} should be mostly less than 30 minutes (Fig. 6a, b). Particles were measured to be semi-solid or amorphous solid in clear days in Beijing (Liu et al., 2017), in Amazonia when influenced by anthropogenic emissions (Bateman et al., 2017), and the boreal forest in Finland (Virtanen et a., 2010). Under these conditions and also when particles are transported to the free troposphere, τ_{eq} can be longer than 1 hour especially in remote areas with low mass loadings (Fig. 6c, d)”.

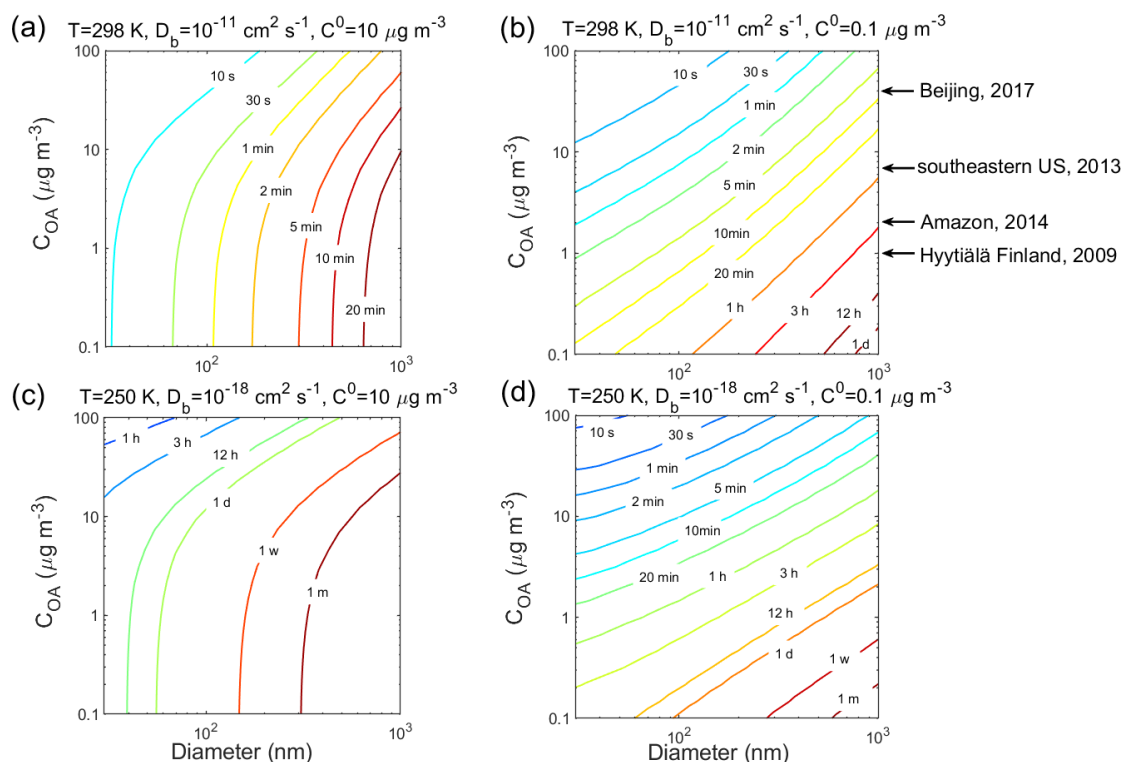


Figure 6. Equilibration timescale (τ_{eq}) for (a, c) SVOC ($C^0 = 10 \mu\text{g m}^{-3}$) and (b, d) LVOC ($C^0 = 0.1 \mu\text{g m}^{-3}$) as a function of particle diameter (nm) and mass concentration ($\mu\text{g m}^{-3}$) of pre-existing particles at 60% RH and T of (a-b) 298 K and (c-d) 250 K in the closed system. The glass transition temperature of pre-existing particles under dry conditions ($T_{g,org}$) is set to be 270 K, which leads to D_b of (a-b) $10^{-11} \text{ cm}^2 \text{ s}^{-1}$ and (c-d) $10^{-18} \text{ cm}^2 \text{ s}^{-1}$. Ambient organic mass concentrations are indicated with arrows.

Referee Minor Comments and Technical Corrections:

(1) Line 89. It is a little confusing here about what temperature was used in the calculations. I wasn't clear whether 273.15 K was used (the most common definition of standard temperature), or if the temperature was variable as a function of pressure altitude. Adding to the confusion, Table S2 lists standard temperature as 288.15 K. Please clarify.

Response: In our simulations the temperature is varied from 220 K to 310 K (Fig. 5) while atmospheric pressure is calculated as a function of T based on the International Standard Atmosphere (ISA): $P/P_{standard} = (T/T_{standard})^{g/LR}$, where $P_{standard}$ and $T_{standard}$ are standard sea level P and T in ISA, and L is the lapse rate of 6.5 K/km in the troposphere. This has been clarified on Lines 94-95 and Table S2 in the revised manuscript.

(2) Lines 108-110. An assumption here is that the organic and aqueous phases are not phase separated. The authors point out later in the manuscript that phase separations may occur, but I suggest also briefly mentioning that phase separation has been observed for laboratory generated SOA (You et al., 2012) here, since it is very relevant to their modeling results.

Response: The following sentence has been added on Lines 116-119 in the revised manuscript:

“For simplicity we assume particles are ideally-mixed, even though phase-separated particles are observed for ambient and laboratory generated SOA particles under certain conditions (You et al., 2012; Renbaum-Wolff et al., 2016)”.

(3) Lines 144 and elsewhere. I found the use of C_0 as an abbreviation more confusing than necessary. It seems C_0 is identical to the much more commonly used C^* . Why not use the commonly accepted C^* ? The authors also use $C_{p,0}$ and $C_{g,0}$, which have a different meaning and cause some confusion with C_0 . Whatever symbol the author use for the saturation vapor pressure please define it the first time it is used.

Response: Instead of C_0 , C^0 , which is commonly used for the pure compound saturation mass concentration, is used throughout the revised manuscript. The effective saturation mass concentration C^* is not used as it includes the effect of non-ideal thermodynamic mixing which is not considered in this study. Lines 154-157 have been re-written in the revised manuscript as:

“Figure 2a presents simulations for a semi-volatile organic compound (SVOC) with the pure compound saturation mass concentration (C^0) of $10 \mu\text{g m}^{-3}$ condensing on particles with D_b of $10^{-11} \text{ cm}^2 \text{ s}^{-1}$ at $\text{RH} = 60\%$ and $T = 298 \text{ K}$ (Fig. S2)”.

(4) Figures 4, A1, A2. The labels on different contours were illegible on the printed document.

Response: The resolution of the figures has been improved in the revised manuscript.

1 **Timescales of Secondary Organic Aerosols to Reach Equilibrium at**
2 **Various Temperatures and Relative Humidities**

3

4 **Ying Li¹, and Manabu Shiraiwa^{1,*}**

5 [1] Department of Chemistry, University of California, Irvine, California, USA.

6

7 *Correspondence to: Manabu Shiraiwa (m.shiraiwa@uci.edu)

8

9 **Abstract:**

10 Secondary organic aerosols (SOA) account for a substantial fraction of air particulate
11 matter and SOA formation is often modeled assuming rapid establishment of
12 gas-particle equilibrium. Here, we estimate the characteristic timescale for SOA to
13 achieve gas-particle equilibrium under a wide range of temperatures and relative
14 humidities using a state-of-the-art kinetic flux model. Equilibration timescales were
15 calculated by varying particle phase state, size, mass loadings, and volatility of
16 organic compounds [in open and closed systems](#). Model simulations suggest that the
17 equilibration timescale for semi-volatile compounds is on the order of seconds or
18 minutes for most conditions in the planetary boundary layer, but it can be longer than
19 one hour if particles adopt glassy or amorphous solid states with high glass transition
20 temperature at low relative humidity. In the free troposphere with lower temperatures
21 it can be longer than hours or days even at moderate or relatively high relative
22 humidity due to kinetic limitations of bulk diffusion in highly viscous particles. The
23 timescale of partitioning of low-volatile compounds [into highly viscous particles](#) is
24 shorter compared to semi-volatile compounds in the closed system, as it is largely
25 determined by condensation sink due to very slow re-evaporation [with relatively](#)
26 [quick establishment of local equilibrium between the gas phase and the near-surface](#)
27 [bulk. The dependence of equilibration timescales on both volatility and bulk](#)
28 [diffusivity](#) provides critical insights into thermodynamic or kinetic treatments of SOA
29 partitioning for accurate predictions of gas- and particle-phase concentrations of
30 semi-volatile compounds in regional and global chemical transport models.

31 **1. Introduction**

32 Secondary organic aerosols (SOA) play a central role in climate, air quality
33 and public health. Accurate descriptions of formation and evolution of SOA remain a
34 grand challenge in climate and air quality models (Kanakidou et al., 2005; Shrivastava
35 et al., 2017a). Current chemical transport models usually employ instantaneous
36 equilibrium partitioning of semi-volatile oxidation products into the particle phase
37 (Pankow, 1994), assuming that SOA partitioning is rapid compared to the timescales
38 of other major atmospheric processes associated with SOA formation. The timescale
39 of SOA to reach equilibrium with their surrounding condensable vapors needs to be
40 evaluated under different ambient conditions to validate this assumption.

41 SOA particles can adopt liquid (dynamic viscosity $\eta < 10^2$ Pa s), semi-solid
42 ($10^2 \leq \eta \leq 10^{12}$ Pa s), or glassy or amorphous solid states ($\eta > 10^{12}$ Pa s), depending
43 on chemical composition, temperature (T) and relative humidity (RH) (Virtanen et al.,
44 2010; Koop et al., 2011; Zhang et al., 2015; Reid et al., 2018). The occurrence of
45 glassy or amorphous solid states may lead to kinetic limitations and prolonged
46 equilibration timescale in SOA partitioning (Shiraiwa and Seinfeld, 2012; Booth et
47 al., 2014; Zaveri et al., 2014; Mai et al., 2015), affecting evolution of particle size
48 distribution upon SOA growth (Maria et al., 2004; Shiraiwa et al., 2013a; Zaveri et
49 al., 2018). A number of experimental studies have indeed observed kinetic limitations
50 of the bulk diffusion of organic molecules (Vaden et al., 2011; Perraud et al., 2012;
51 Ye et al., 2016a; Zhang et al., 2018), while chamber experiments probing the

52 intraparticle mixing did not find kinetic limitations at moderate and high RH and
53 room temperature (Ye et al., 2016b; Gorkowski et al., 2017; Ye et al., 2018).

54 Recently, global simulations predicted that SOA particles are expected to be
55 mostly in a glassy solid phase state in the middle and upper troposphere and also in
56 dry lands in the boundary layer (Shiraiwa et al., 2017), which can lead to prolonged
57 characteristic bulk diffusion timescales of organic molecules within SOA particles
58 (Shiraiwa et al., 2011; Maclean et al., 2017). Slow bulk diffusion associated with a
59 glassy phase state can prevent atmospheric oxidants to react with organic compounds
60 such as polycyclic aromatic hydrocarbons (Shrivastava et al., 2017b; Mu et al., 2018),
61 contributing to long-range transport of organic compounds. Recent ambient
62 observations have shown that the condensation of highly oxygenated molecules
63 (HOMs), which play an important role in new particle formation, would be governed
64 by kinetic partitioning in the free troposphere (Bianchi et al., 2016). Diffusivity
65 measurements of volatile organics in levitated viscous particles have shown strong
66 temperature dependence of bulk diffusivity and evaporation timescale (Bastelberger et
67 al., 2017). Slow bulk diffusion may impact multiphase processes such as browning of
68 organic particles (Liu et al., 2018), cloud droplet activation (Slade et al., 2017), and
69 ice nucleation pathways (Knopf et al., 2018).

70 Given these observations and strong implications of SOA phase states, it is
71 important to evaluate common assumption of gas-particle partitioning equilibrium at
72 different ambient conditions. In this study we provide theoretical analysis of
73 partitioning kinetics of organic compounds using the kinetic multi-layer model of

74 gas-particle interactions in aerosols and clouds (KM-GAP) (Shiraiwa et al., 2012),
75 which accounts for mass transport in both gas and particle phases. The equilibration
76 timescale (τ_{eq}) of organic compounds partitioning into mono-dispersed particles is
77 evaluated systematically under a wide range of temperatures and RH, considering the
78 effects of particle phase state, particle size, mass loadings, and volatility of organic
79 compounds in a closed system with finite amount of vapor. For comparison we also
80 present simulations in an open system with vapor concentration maintained as
81 constant. This is the first study to directly relate equilibration timescale of SOA
82 partitioning to ambient temperature and relative humidity, which has important
83 implications in treatment of SOA evolution in chemical transport models.

84

85 **2. Methods**

86 We evaluate the timescale to achieve gas-particle equilibrium by simulating
87 condensation of a compound Z into pre-existing non-volatile mono-dispersed particles
88 using the KM-GAP model. KM-GAP consists of multiple model compartments and
89 layers, respectively: gas phase, near-surface gas phase, sorption layer, surface layer,
90 and a number of bulk layers (Shiraiwa et al., 2012). The following processes are
91 treated as temperature-dependent in KM-GAP: gas phase diffusion,
92 adsorption/desorption, surface-bulk exchange, and bulk diffusion (Fig. S1). The
93 physical and kinetic parameters are summarized in Table S1. The gas-phase diffusion
94 coefficient depends on temperature (T) and ambient pressure (P). P is calculated as a
95 function of T based on the International Standard Atmosphere

96 (<https://www.iso.org/standard/7472.html>). The adsorption rate coefficient is related to
97 the mean thermal velocity as a function of T and the surface accommodation
98 coefficient, which is assumed to be 1 (Julin et al., 2014). The T -dependence of
99 desorption rate coefficient is described by an Arrhenius equation with an assumed
100 typical adsorption enthalpy of 40 kJ mol^{-1} .

101 Phase state and viscosity can be characterized by the glass transition
102 temperature (T_g), at which phase transition between amorphous solid and semi-solid
103 states occurs (Koop et al., 2011). When T_g of organic particles under dry conditions
104 ($T_{g,org}$) is known, T_g of organic-water mixtures at given RH can be estimated
105 considering hygroscopic growth combined with the Gordon-Taylor equation. In this
106 work, we assumed the effective hygroscopicity parameter as 0.1 (Petters and
107 Kreidenweis, 2007; Gunthe et al., 2009) and the Gordon-Taylor constant as 2.5 (Koop
108 et al., 2011). Then, the T -dependence of viscosity is calculated using the
109 Vogel-Tammann-Fulcher equation (Angell, 1991; Rothfuss and Petters, 2017;
110 DeRieux et al., 2018; Li and Shiraiwa, 2018).

111 Figure 1 shows the T - and RH-dependent viscosity of SOA particles with $T_{g,org}$
112 of (a) 240 K, (b) 270 K, and (c) 300 K. We chose these three $T_{g,org}$ values to represent
113 different phase states of liquid, semi-solid, and glassy states, respectively, at T of 298
114 K under dry conditions and these values are within the range recently reported for
115 monoterpene-derived SOA (Petters et al., 2019). The decrease of T leads to increase
116 of viscosity, while the increase of RH leads to decrease of viscosity due to the
117 plasticizing effect of water (Koop et al., 2011). For simplicity we assume particles are

118 ideally-mixed, even though phase-separated particles are observed for ambient and
119 laboratory generated SOA particles under certain conditions (You et al., 2012;
120 Renbaum-Wolff et al., 2016). The bulk diffusion coefficient D_b (Fig. S2) is calculated
121 by the Stokes–Einstein equation, which has been shown to work very well for organic
122 molecules diffusing through materials with viscosity below $\sim 10^3$ Pa s (Chenyakin et
123 al., 2017). Note that the Stokes–Einstein equation may underpredict D_b in highly
124 viscous SOA thus it gives lower limits of D_b (Price et al., 2015; Marshall et al., 2016;
125 Bastelberger et al., 2017; Reid et al., 2018). D_b is fixed at any given depth in the
126 particle bulk in each simulation, assuming that condensation of Z would not alter
127 particle viscosity and diffusivity as only trace amounts of Z condense to pre-existing
128 particles in our simulations. Particle-phase reactions and their potential impacts on
129 particle viscosity are also not considered in this study.

130 We mainly consider a closed system, in which condensation of Z would lead
131 to a decrease of its gas-phase mass concentration (C_g) and an increase of its
132 particle-phase mass concentration (C_p). The particle diameter stays practically
133 constant throughout each simulation, as the amount of condensing Z is set to be much
134 smaller than the non-volatile pre-existing particle mass (C_{OA}). The gas-phase mass
135 concentration of Z right above the surface (C_s) is also calculated based on the Raoult’s
136 law and partitioning theory (Pankow, 1994) in equilibrium with the near-surface bulk,
137 which is resolved by KM-GAP (Shiraiwa and Seinfeld, 2012). We also calculate the
138 mass fraction of Z in the near-surface bulk (f_s) and the average mass fraction of Z in

139 the entire bulk (f_b) to infer the radial concentration profile (Fig. S3). The equilibration
140 timescale (τ_{eq}) is calculated as the e-folding time t when the following criterion is met,

$$141 \quad \frac{|C_p(t) - C_{p,eq}|}{|C_{p,0} - C_{p,eq}|} < \frac{1}{e} \quad (1)$$

142 where $C_{p,0}$ and $C_{p,eq}$ are the initial and equilibrium mass concentration of Z in the
143 particle phase, respectively. Note that practically the same values can also be obtained
144 by using initial and equilibrium gas-phase concentrations in Eq. (1), as the mass
145 change of Z in the gas and particle phases are the same in these simulations.

146

147 **3 Results**

148 **3.1. Impacts of volatility and diffusivity on equilibration timescales**

149 Figure 2 shows exemplary simulations of temporal evolution of C_g (blue line)
150 and C_p (red line) of the compound Z in the closed system along with τ_{eq} marked with
151 red circles. The initial mass concentration of pre-existing non-volatile mono-dispersed
152 particles (C_{OA}) is assumed to be $20 \mu\text{g m}^{-3}$ with the number concentrations of 3×10^4
153 cm^{-3} and the initial particle diameter of 100 nm. Initial mass concentrations of Z in the
154 gas ($C_{g,0}$) and particle ($C_{p,0}$) phases are set to be $0.3 \mu\text{g m}^{-3}$ and $0 \mu\text{g m}^{-3}$, respectively.
155 $T_{g,org}$ is assumed to be 270 K. Figure 2a presents simulations for a semi-volatile
156 organic compound (SVOC) with the pure compound saturation mass concentration
157 (C^0) of $10 \mu\text{g m}^{-3}$ condensing on particles with D_b of $10^{-11} \text{cm}^2 \text{s}^{-1}$ at RH = 60% and T
158 = 298 K (Fig. S2). Upon condensation C_g decreases, while C_s and C_p increase, and the
159 gas-particle equilibrium is reached within about 20 s as indicated by τ_{eq} . For
160 low-volatile organic compounds (LVOC) with $C^0 = 0.1 \mu\text{g m}^{-3}$, it takes longer time to

161 reach the equilibrium with τ_{eq} of ~ 30 s (Fig. 2b), as the partial pressure gradient
162 between the gas phase and the particle surface (represented by the difference between
163 C_{g} and C_{s}) is larger for lower C^0 . For both cases SOA growth is governed by
164 gas-phase diffusion as indicated by $C_{\text{s}} < C_{\text{g}}$. The mass fraction of Z in the near-surface
165 bulk is identical to the average mass fraction in the entire bulk (Fig. S3 a–b),
166 indicating that Z are homogeneously well-mixed in the particle without kinetic
167 limitations of bulk diffusion in low viscous particles (Fig. 3a).

168 At lower T of 250 K, the phase state of pre-existing particles occurs as highly
169 viscous with D_{b} of $\sim 10^{-18}$ $\text{cm}^2 \text{s}^{-1}$ (Fig. S2), resulting in much longer equilibration
170 timescales ($\sim 10^5$ s) for SVOC with $C^0 = 10 \mu\text{g m}^{-3}$ (Fig. 2c). After C_{g} and C_{s}
171 converge, they continue to decrease simultaneously while C_{p} increases slowly,
172 showing that the particle undergoes quasi-equilibrium growth (Shiraiwa and Seinfeld,
173 2012; Zhang et al., 2012). For LVOC ($C^0 = 0.1 \mu\text{g m}^{-3}$) condensation, τ_{eq} is short
174 (~ 140 s) because of a local thermodynamic equilibrium between the gas phase and the
175 near-surface bulk established relatively quickly (as mostly controlled by the
176 condensation sink: Riipinen et al., 2011; Tröstl et al., 2016) due to very slow
177 re-evaporation of LVOC.

178 The characteristic timescale of mass transport and mixing by molecular
179 diffusion τ_{mix} can be calculated by $\tau_{\text{mix}} = r_{\text{p}}^2 / (\pi^2 D_{\text{b}})$, where r_{p} is the particle radius
180 (Seinfeld and Pandis, 2006). Figure 3 shows dimensionless radial concentration
181 profiles of Z ($C^0 = 0.1 \mu\text{g m}^{-3}$) in the particle at (a) $D_{\text{b}} = 10^{-11}$ $\text{cm}^2 \text{s}^{-1}$ and (b) 10^{-18} cm^2
182 s^{-1} , respectively. For low viscous particles, τ_{mix} is very short and particles are

183 homogeneously well-mixed at τ_{eq} , which is consistent with previous analytical
184 calculations (Liu et al., 2013; Mai et al., 2015). In contrast, there exists a large
185 concentration gradient between the particle surface and the inner bulk (Fig. 3b, S3d)
186 at τ_{eq} in highly viscous particles due to strong kinetic limitations of bulk diffusion (as
187 indicated by very long τ_{mix}), which prevents the entire particle bulk to reach complete
188 equilibrium. Thus, for LVOC condensation on highly viscous particles (Fig. 2d), τ_{mix}
189 represents the timescale to establish full equilibrium with homogeneous mixing in the
190 entire particle bulk. These results are consistent with Mai et al. (2015) and Liu et al.
191 (2016), which showed that an establishment of full equilibrium is limited by bulk
192 diffusion in highly viscous particles, even though the local equilibrium of LVOC may
193 be achieved faster. Note that τ_{mix} is solely a function of particle size and bulk
194 diffusivity, while τ_{eq} is also affected by volatility and mass loadings. At lower particle
195 concentrations, the total accommodation of molecules to the particle surface
196 decreases, resulting in longer equilibration timescales (Fig. S4).

197 We further computed τ_{eq} as a function of D_b and C^0 in the closed system. As
198 shown in Fig. 4a, when D_b is higher than $\sim 10^{-13} \text{ cm}^2 \text{ s}^{-1}$, τ_{eq} is insensitive to bulk
199 diffusivity but sensitive to volatility: decreasing volatility increases τ_{eq} in this regime.
200 In the regime with D_b lower than $\sim 10^{-13} \text{ cm}^2 \text{ s}^{-1}$ and C^0 higher than $\sim 10 \mu\text{g m}^{-3}$, τ_{eq} is
201 controlled by bulk diffusivity: τ_{eq} increases from 30 s to longer than 1 year as D_b
202 decreases from $10^{-13} \text{ cm}^2 \text{ s}^{-1}$ to $10^{-20} \text{ cm}^2 \text{ s}^{-1}$. In the regime with $D_b < \sim 10^{-13} \text{ cm}^2 \text{ s}^{-1}$
203 and $C^0 < \sim 10 \mu\text{g m}^{-3}$, τ_{eq} depends on both diffusivity and volatility. Decreasing

204 volatility would lead to shorter τ_{eq} due to an establishment of local equilibrium of
205 LVOC.

206 In an open system with fixed vapor concentration (Fig. S5), τ_{eq} of SVOC is
207 slightly longer but on the same order of magnitude as τ_{eq} in the closed system, as
208 relatively small amounts of SVOC need to condense to reach equilibrium. In contrast,
209 τ_{eq} of LVOC in the open system become dramatically longer as LVOC continue to
210 condense into the particle phase because of low volatility (Pankow, 1994). For further
211 simulations we focus mainly on the closed system and the corresponding simulations
212 for the open system are provided in the supplement.

213 We also simulated evaporation in the closed system with same parameters as
214 the condensation simulations (Table S2). Initially $C_{\text{g}} = 0 \mu\text{g m}^{-3}$ and trace amounts of
215 semi-volatile or low-volatile species were assumed to be homogeneously well-mixed
216 in pre-existing particles. Figure S6 shows that for the evaporation of SVOC species
217 with $C^0 = 10 \mu\text{g m}^{-3}$, decreasing D_{b} from $10^{-11} \text{ cm}^2 \text{ s}^{-1}$ to $10^{-18} \text{ cm}^2 \text{ s}^{-1}$ would increase
218 τ_{eq} from $\sim 20 \text{ s}$ to $\sim 10^5 \text{ s}$. These evaporation timescales are close to those derived
219 from condensation (Fig. 2a,c) and consistent with previous kinetic simulations (Liu et
220 al., 2016). In the closed system, the evaporation of a very small amount of LVOC
221 species from the particle surface is already sufficient to reach the particle-phase
222 equilibrium concentration, resulting in a short τ_{eq} (Fig. S6b,d). For an open system
223 with continuous removal of gas-phase compounds, which is often employed in
224 evaporation experiments, the equilibrium timescale in the evaporation of the LVOC
225 species from highly viscous particles can be longer than hours or days (Vaden et al.,

226 2011; Liu et al., 2016). Figure 4b shows simulated evaporation timescales as a
227 function of D_b and C^0 in an open system, which agrees very well with Fig. 3 in Liu et
228 al. (2016). It shows that for less viscous particles τ_{eq} is limited by volatility, while for
229 highly viscous particles τ_{eq} is insensitive to volatility and controlled by bulk
230 diffusivity.

231

232 3.2. Equilibration timescales at different RH and T

233 We conducted further simulations to estimate τ_{eq} with a wide range of
234 atmospherically-relevant temperatures (220 - 310 K) and relative humidities (0 -
235 100%). Figure 5 shows the temperature and humidity-dependent diagrams of τ_{eq} for
236 SVOC ($C^0 = 10 \mu\text{g m}^{-3}$) condensation on particles with $T_{g,org}$ of 240 K, 270 K, and
237 300 K, respectively, in the closed system. For particles with $T_{g,org}$ of 240 K (panel a),
238 τ_{eq} is on the order of seconds under boundary layer conditions ($T > 270$ K). In these
239 conditions particles are liquid with high bulk diffusivity (Fig. 1a and S2a), thus
240 gas-particle partitioning is controlled by gas-phase diffusion and interfacial transport
241 (Shiraiwa and Seinfeld, 2012; Mai et al., 2015). At low T (< 260 K) with low or
242 moderate RH ($< 70\%$), τ_{eq} can increase from minutes to one year with decreasing T
243 and RH mainly due to strong kinetic limitations of bulk diffusion with low D_b (Fig.
244 S2a). With $T_{g,org}$ of 270 K (panel b) or 300 K (panel c), τ_{eq} is still on the order of
245 minutes in most of boundary layer conditions. At low RH τ_{eq} can be extended to hours
246 when particles may occur as amorphous (semi-)solid. When $T < 270$ K, τ_{eq} can be
247 longer than months even at moderate RH, while τ_{eq} may stay very short at very high

248 RH. The corresponding simulations of SVOC partitioning in the open system (Fig.
249 S7) show a similar pattern as τ_{eq} in the closed system.

250 τ_{eq} for $C^0 = 10^3$ and $0.1 \mu\text{g m}^{-3}$ in the closed system are presented in Fig. A1. In
251 general, τ_{eq} would be shorter at higher C^0 when particles are liquid, as the partial
252 pressure gradient between the gas phase and the particle surface is smaller for higher
253 C^0 (Shiraiwa and Seinfeld, 2012; Liu et al., 2016). For example, the increase of C^0
254 from $10 \mu\text{g m}^{-3}$ to $10^3 \mu\text{g m}^{-3}$ leads to τ_{eq} decrease from 30 s to 1 s with $T_{\text{g,org}}$ of 240 K
255 at boundary layer conditions (Fig. 5a, A1a). At low T and RH (e.g., $T < 250$ K and
256 $\text{RH} < 50\%$) where particles are highly viscous, τ_{eq} is on the same order of magnitude
257 for the condensation of IVOC and SVOC, as gas-particle partitioning is limited by
258 bulk diffusion. Figure A2 shows bulk diffusion and mixing timescales (τ_{mix}) as a
259 function of RH and T . It is interesting to note that τ_{mix} is very similar to τ_{eq} of IVOC
260 (Fig. A1(a-c)) as gas diffusion and interfacial transport of IVOC are fast. For LVOC
261 τ_{eq} is generally shorter than τ_{mix} as its mass transfer to the particle surface is governed
262 by condensation sink with negligible re-evaporation, while τ_{mix} is still long to achieve
263 homogeneous mixing in the particle phase if particles are viscous.

264 Previous studies have shown that τ_{eq} depends on particle size (Liu et al., 2013;
265 Zaveri et al., 2014; Mai et al., 2015) and particle mass loadings (Shiraiwa and
266 Seinfeld, 2012; Saleh et al., 2013). For further examination of these effects at
267 different T , Figure 6 shows the dependence of τ_{eq} of SVOC ($C^0 = 10 \mu\text{g m}^{-3}$) and
268 LVOC ($C^0 = 0.1 \mu\text{g m}^{-3}$) on the mass concentration and the diameter of pre-existing
269 particles, over the range of $0.1 - 100 \mu\text{g m}^{-3}$ and $30 - 1000$ nm, respectively, with

270 particle phase state to be less viscous with $D_b = 10^{-11} \text{ cm}^2 \text{ s}^{-1}$ at 298 K and highly
271 viscous with $D_b = 10^{-18} \text{ cm}^2 \text{ s}^{-1}$ at 250 K. In this comparison, when ambient particle
272 mass concentration is held constant, increasing particle size will translate to a
273 decrease of the number and surface area concentration of particles, and a decrease of
274 total accommodation of molecules to the particle surface, thereby leading to an
275 increase of τ_{eq} . When particle diameter is held constant, an increase of particle
276 concentration leads to an increase of surface area concentration, resulting in shorter
277 τ_{eq} . When particles are less viscous at 298 K ($D_b = 10^{-11} \text{ cm}^2 \text{ s}^{-1}$) τ_{eq} of SVOC is
278 shorter than that of LVOC for the same particle size and mass loadings. For
279 partitioning into highly viscous particles at 250 K ($D_b = 10^{-18} \text{ cm}^2 \text{ s}^{-1}$), SVOC takes
280 longer time than LVOC to reach equilibrium.

281 Typical ambient organic mass concentrations in Beijing, Centreville in
282 southeastern US, Amazon Basin, and Hyytiälä, Finland are indicated in Fig. 6. The
283 particle phase state was observed to be mostly liquid in highly polluted episodes in
284 Beijing (Liu et al., 2017), under typical atmospheric conditions in the southeastern US
285 (Pajunoja et al., 2016), and under background conditions in Amazonia (Bateman et
286 al., 2017). At these conditions τ_{eq} should be mostly less than 30 minutes (Fig. 6a, b).
287 Particles were measured to be semi-solid or amorphous solid in clear days in Beijing
288 (Liu et al., 2017), in Amazonia when influenced by anthropogenic emissions
289 (Bateman et al., 2017), and the boreal forest in Finland (Virtanen et a., 2010). Under
290 these conditions and also when particles are transported to the free troposphere, τ_{eq}
291 can be longer than 1 hour especially in remote areas with low mass loadings (Fig. 6c,

292 d). Particles in nucleation mode (diameter < 30 nm) are not considered in this study,
293 as the particle size may affect the phase transition of these nanoparticles (Cheng et al.,
294 2015). The role and impact of phase transition on nucleation and growth of ultrafine
295 particles are beyond the scope of current simulations and need further investigations
296 in future studies.

297

298 **4 Discussion**

299 The timescale to reach equilibrium for SOA partitioning has been investigated
300 in several laboratory experiments at room temperatures (Vaden et al., 2011; Saleh et
301 al., 2013; Liu et al., 2016; Ye et al., 2016a; Gong et al., 2018; Ye et al., 2018). These
302 experiments monitored particle mass or composition, finding that equilibration
303 timescales are longer at low RH, consistent with our model simulations. Note that, for
304 condensation on highly viscous particles, even though particle mass or particle-phase
305 concentrations appear to reach equilibrium, complete equilibrium with homogeneous
306 mixing in the particle may not have been reached driven by strong kinetic limitations
307 and concentration gradients in the particle bulk (Fig. 2d and 3b). This is also
308 supported by evaporation experiments showing that the local thermodynamic
309 equilibrium established between the vapor and the near-surface bulk should be
310 differentiated from the global equilibrium between the vapor and the entire bulk (Liu
311 et al., 2016). Note that SOA evaporation is also influenced by volatility and oligomer
312 decomposition (Roldin et al., 2014; Yli-Juuti et al., 2017). The timescale of
313 gas-particle partitioning can be different in closed or open systems especially for

314 LVOC (Fig. 4, S7). The closed system simulations represent SOA partitioning in
315 chamber experiments and in closed atmospheric air mass, which could be justified
316 well within seconds-to-minutes timescales and possibly up to hours depending on
317 meteorological conditions. The real atmosphere may be approximated better as an
318 open system due to dilution and chemical production and loss especially at longer
319 timescales. Thus, particular care needs to be taken in comparing modeling results with
320 different field conditions or experiments on probing equilibration timescale (i.e.,
321 evaporation vs. condensation, open vs. closed system, local vs. full equilibrium).

322 The simulated equilibration timescales of atmospheric SOA are mostly on the
323 order of minutes to hours under conditions of atmospheric boundary layer (Fig. 5,
324 A1). This agrees with previous experimental results that the gas-particle interactions
325 can be regulated by both thermodynamic and kinetic partitioning (Booth et al., 2014;
326 Liu et al., 2016; Saha and Grieshop, 2016; Ye et al., 2016a; Gong et al., 2018),
327 depending on several factors including particle phase state, size, mass loadings, and
328 volatility. Organic particles containing high molar-mass compounds tend to have high
329 glass transition temperatures (Koop et al., 2011) and the occurrence of kinetic
330 limitation will increase with higher $T_{g,org}$ (Fig. 5). This is consistent with the results of
331 intraparticle mixing experiments showing that as the carbon number of precursor (e.g.
332 terpene) increased (that would lead to higher $T_{g,org}$), it took longer time for SVOCs
333 (evaporated from another type of SOA, e.g. toluene SOA) to partition into the terpene
334 SOA, leading to slower molecular exchange among different types of SOA (Ye et al.,
335 2018).

336 At low temperatures, the particles can occur as highly viscous at relatively
337 high RH (Fig. 1), and τ_{eq} of SVOC partitioning can be longer than hours or days (Fig.
338 5, S7). Equilibration timescales of LVOC condensation at low particle mass loadings
339 (Fig. 6) may represent the clean conditions where new particle formation and growth
340 often occur (Wang et al., 2016). It has been reported that highly oxygenated
341 molecules play an important role in the initial growth of atmospheric particles in the
342 free troposphere (Bianchi et al., 2016). Bulk diffusion would likely to be a limiting
343 step in the condensation of semi-volatile and low volatility compounds at low
344 temperatures, where particles may occur as highly viscous (Shiraiwa et al., 2017). In
345 this case, particle growth would need to be treated kinetically, rather than
346 thermodynamic equilibrium partitioning, as it would affect SOA growth kinetics and
347 size distribution dynamics, with significant implications for the growth of ultrafine
348 particles to climatically relevant sizes (Riipinen et al., 2011; Riipinen et al., 2012;
349 Shiraiwa et al., 2013a; Zaveri et al., 2018). Chemical transport models usually have
350 time steps on the order of minutes, within which the partitioning equilibrium may not
351 be reached, for most SVOC species ($C^0 > 1 \mu\text{g m}^{-3}$) when D_b is less than $10^{-15} \text{ cm}^2 \text{ s}^{-1}$
352 (Fig. 4). Note that condensation of extremely low volatility organic compounds
353 (ELVOC; Tröstl et al., 2016) into highly viscous particles may be governed by
354 gas-phase diffusion and timescales to reach local equilibrium could be shorter as
355 determined by the condensation sink (Riipinen et al., 2011) (see also Fig. S4b), which
356 may be more relevant for the practical application in chemical transport models.

357 In this study we assume that the bulk diffusivity within organic particles is
358 independent of particle mixing state and morphology. Chamber experiments have
359 demonstrated that evaporation of organic aerosol may be hindered if it is coated with
360 organic aerosol from a different precursor (Loza et al., 2013; Boyd et al., 2017).
361 Moreover, the phase separation has been observed in organic particles mixed with
362 inorganic salts (You et al., 2014) and even without inorganic salts (Pöhlker et al.,
363 2012; Riedel et al., 2016). Future simulations on equilibration timescale should
364 consider the effects of the immiscibility (Barsanti et al., 2017; Liu et al., 2013) and
365 the phase separation (Shiraiwa et al., 2013b; Pye et al., 2017; Fowler et al., 2018) as
366 well as composition-dependent bulk diffusivity (O'Meara et al., 2016) and the
367 evolution of the particle phase due to reactive uptake and condensed-phase chemistry
368 (Hosny et al., 2016). Incorporation of the particle-phase formation of oligomers and
369 other multifunctional high molar mass compounds can lead to a reduced bulk
370 diffusivity (Pfrang et al., 2011; Hosny et al., 2016), which may prolong the
371 equilibration timescales. Decomposition of highly oxidized molecules (e.g., organic
372 hydroperoxides) in water may also affect gas-particle partitioning (Tong et al., 2016).
373 Current simulations are focused on trace amount of SVOC or LVOC condensing on
374 mono-dispersed particles with negligible particle growth. Potential phase transition in
375 the course of particle growth/evaporation should also be incorporated in future
376 simulations. The shift in particle phase state and gas-particle partitioning in response
377 to temperature and RH may need to be considered in chemical transport models and
378 laboratory experiments to better understand the fate of organic compounds.

379

380 **Author contribution.**

381 YL and MS designed and conducted modeling and wrote the manuscript.

382

383 **Acknowledgments.**

384 This work was funded by the National Science Foundation (AGS-1654104) and the
385 Department of Energy (DE-SC0018349). The simulation data may be obtained from
386 the corresponding author upon request.

387

388 **References**

- 389 Angell, C.: Relaxation in liquids, polymers and plastic crystals—strong/fragile
390 patterns and problems, *J. Non-Cryst. Solids*, 131-133, 13-31,
391 [https://doi.org/10.1016/0022-3093\(91\)90266-9](https://doi.org/10.1016/0022-3093(91)90266-9), 1991.
- 392 Barsanti, K. C., Kroll, J. H. and Thornton, J. A.: Formation of low-volatility organic
393 compounds in the atmosphere: recent advancements and insights, *J. Phys.*
394 *Chem. Lett.*, 8, 1503-1511, <https://doi.org/10.1021/acs.jpcclett.6b02969>, 2017.
- 395 Bastelberger, S., Krieger, U. K., Luo, B. and Peter, T.: Diffusivity measurements of
396 volatile organics in levitated viscous aerosol particles, *Atmos. Chem. Phys.*,
397 17, 8453-8471, <https://doi.org/10.5194/acp-17-8453-2017>, 2017.
- 398 Bateman, A. P., Gong, Z., Harder, T. H., de Sá, S. S., Wang, B., Castillo, P., China,
399 S., Liu, Y., O'Brien, R. E., Palm, B. B., Shiu, H. W., Cirino, G. G., Thalman,
400 R., Adachi, K., Alexander, M. L., Artaxo, P., Bertram, A. K., Buseck, P. R.,
401 Gilles, M. K., Jimenez, J. L., Laskin, A., Manzi, A. O., Sedlacek, A., Souza,
402 R. A. F., Wang, J., Zaveri, R. and Martin, S. T.: Anthropogenic influences on
403 the physical state of submicron particulate matter over a tropical forest,
404 *Atmos. Chem. Phys.*, 17, 1759-1773,
405 <https://doi.org/10.5194/acp-17-1759-2017>, 2017.
- 406 Bianchi, F., Tröstl, J., Junninen, H., Frege, C., Henne, S., Hoyle, C. R., Molteni, U.,
407 Herrmann, E., Adamov, A., Bukowiecki, N., Chen, X., Duplissy, J., Gysel,
408 M., Hutterli, M., Kangasluoma, J., Kontkanen, J., Kürten, A., Manninen, H.
409 E., Münch, S., Peräkylä, O., Petäjä, T., Rondo, L., Williamson, C.,
410 Weingartner, E., Curtius, J., Worsnop, D. R., Kulmala, M., Dommen, J. and
411 Baltensperger, U.: New particle formation in the free troposphere: A question

412 of chemistry and timing, *Science*, 352, 1109-1112,
413 <https://doi.org/10.1126/science.aad5456>, 2016.

414 Booth, A. M., Murphy, B., Riipinen, I., Percival, C. J. and Topping, D. O.:
415 Connecting bulk viscosity measurements to kinetic limitations on attaining
416 equilibrium for a model aerosol composition, *Environ. Sci. Technol.*, 48,
417 9298-9305, <https://doi.org/10.1021/es501705c>, 2014.

418 Boyd, C. M., Nah, T., Xu, L., Berkemeier, T. and Ng, N. L.: Secondary organic
419 aerosol (SOA) from nitrate radical oxidation of monoterpenes: effects of
420 temperature, dilution, and humidity on aerosol formation, mixing, and
421 evaporation, *Environ. Sci. Technol.*, 51, 7831-7841,
422 <https://doi.org/10.1021/acs.est.7b01460>, 2017.

423 Cheng, Y., Su, H., Koop, T., Mikhailov, E. and Pöschl, U.: Size dependence of phase
424 transitions in aerosol nanoparticles, *Nat. Commun.*, 6, 5923,
425 <https://doi.org/10.1038/ncomms6923>, 2015.

426 Chenyakin, Y., Ullmann, D. A., Evoy, E., Renbaum-Wolff, L., Kamal, S. and
427 Bertram, A. K.: Diffusion coefficients of organic molecules in sucrose–water
428 solutions and comparison with Stokes–Einstein predictions, *Atmos. Chem.
429 Phys.*, 17, 2423-2435, <https://doi.org/10.5194/acp-17-2423-2017>, 2017.

430 DeRieux, W. S. W., Li, Y., Lin, P., Laskin, J., Laskin, A., Bertram, A. K.,
431 Nizkorodov, S. A. and Shiraiwa, M.: Predicting the glass transition
432 temperature and viscosity of secondary organic material using molecular
433 composition, *Atmos. Chem. Phys.*, 18, 6331-6351,
434 <https://doi.org/10.5194/acp-18-6331-2018>, 2018.

435 Fowler, K., Connolly, P. J., Topping, D. O. and O'Meara, S.: Maxwell–Stefan
436 diffusion: a framework for predicting condensed phase diffusion and phase
437 separation in atmospheric aerosol, *Atmos. Chem. Phys.*, 18, 1629-1642,
438 <https://doi.org/10.5194/acp-18-1629-2018>, 2018.

439 Gong, Z., Han, Y., Liu, P., Ye, J., Keutsch, F. N., McKinney, K. A. and Martin, S. T.:
440 Influence of particle physical state on the uptake of medium-sized organic
441 molecules, *Environ. Sci. Technol.*, 52, 8381-8389,
442 <https://doi.org/10.1021/acs.est.8b02119>, 2018.

443 Gorkowski, K., Donahue, N. M. and Sullivan, R. C.: Emulsified and liquid–liquid
444 phase-separated states of α -pinene secondary organic aerosol determined using
445 aerosol optical tweezers, *Environ. Sci. Technol.*, 51, 12154-12163,
446 <https://doi.org/10.1021/acs.est.7b03250>, 2017.

447 Gunthe, S. S., King, S. M., Rose, D., Chen, Q., Roldin, P., Farmer, D. K., Jimenez, J.
448 L., Artaxo, P., Andreae, M. O., Martin, S. T. and Pöschl, U.: Cloud
449 condensation nuclei in pristine tropical rainforest air of Amazonia:
450 size-resolved measurements and modeling of atmospheric aerosol composition
451 and CCN activity, *Atmos. Chem. Phys.*, 9, 7551-7575,
452 <https://doi.org/10.5194/acp-9-7551-2009>, 2009.

453 Hosny, N., Fitzgerald, C., Vyšniauskas, A., Athanasiadis, A., Berkemeier, T., Uygur,
454 N., Pöschl, U., Shiraiwa, M., Kalberer, M., Pope, F. and Kuimova, M. K.:
455 Direct imaging of changes in aerosol particle viscosity upon hydration and

456 chemical aging, *Chem. Sci.*, 7, 1357-1367,
457 <https://doi.org/10.1039/C5SC02959G>, 2016.

458 Julin, J., Winkler, P. M., Donahue, N. M., Wagner, P. E. and Riipinen, I.: Near-unity
459 mass accommodation coefficient of organic molecules of varying structure,
460 *Environ. Sci. Technol.*, 48, 12083-12089, <https://doi.org/10.1021/es501816h>,
461 2014.

462 Kanakidou, M., Seinfeld, J. H., Pandis, S. N., Barnes, I., Dentener, F. J., Facchini, M.
463 C., Van Dingenen, R., Ervens, B., Nenes, A., Nielsen, C. J., Swietlicki, E.,
464 Putaud, J. P., Balkanski, Y., Fuzzi, S., Horth, J., Moortgat, G. K.,
465 Winterhalter, R., Myhre, C. E. L., Tsigaridis, K., Vignati, E., Stephanou, E. G.
466 and Wilson, J.: Organic aerosol and global climate modelling: a review,
467 *Atmos. Chem. Phys.*, 5, 1053-1123, <https://doi.org/10.5194/acp-5-1053-2005>,
468 2005.

469 Knopf, D. A., Alpert, P. A. and Wang, B.: The role of organic aerosol in atmospheric
470 ice nucleation: a review, *ACS Earth Space Chem.*, 2, 168-202,
471 <https://doi.org/10.1021/acsearthspacechem.7b00120>, 2018.

472 Koop, T., Bookhold, J., Shiraiwa, M. and Poschl, U.: Glass transition and phase state
473 of organic compounds: dependency on molecular properties and implications
474 for secondary organic aerosols in the atmosphere, *Phys. Chem. Chem. Phys.*,
475 13, 19238-19255, <https://doi.org/10.1039/C1CP22617G>, 2011.

476 Li, Y. and Shiraiwa, M.: Molecular corridors, volatility and particle phase state in
477 secondary organic aerosols, in: *Multiphase Environmental Chemistry in the
478 Atmosphere*, edited by: Hunt S. W., Laskin A., and Nizkorodov S. A., ACS
479 Symposium Series, 1299, 209-244,
480 <https://doi.org/10.1021/bk-2018-1299.ch011>, 2018.

481 Liu, C., Shi, S., Weschler, C., Zhao, B. and Zhang, Y.: Analysis of the dynamic
482 interaction between SVOCs and airborne particles, *Aerosol Sci. Technol.*, 47,
483 125-136, <https://doi.org/10.1080/02786826.2012.730163>, 2013.

484 Liu, P., Li, Y. J., Wang, Y., Gilles, M. K., Zaveri, R. A., Bertram, A. K. and Martin,
485 S. T.: Lability of secondary organic particulate matter, *Proc. Natl. Acad. Sci.
486 U.S.A.*, 113, 12643-12648, <https://doi.org/10.1021/acscentsci.7b00452>, 2016.

487 Liu, P., Li, Y. J., Wang, Y., Bateman, A. P., Zhang, Y., Gong, Z., Bertram, A. K. and
488 Martin, S. T.: Highly viscous states affect the browning of atmospheric
489 organic particulate matter, *ACS Cent. Sci.*,
490 <https://doi.org/10.1021/acscentsci.7b00452>, 2018.

491 Liu, Y., Wu, Z., Wang, Y., Xiao, Y., Gu, F., Zheng, J., Tan, T., Shang, D., Wu, Y.,
492 Zeng, L., Hu, M., Bateman, A. P. and Martin, S. T.: Submicrometer particles
493 are in the liquid state during heavy haze episodes in the urban atmosphere of
494 Beijing, China, *Environ. Sci. Technol. Lett.*, 4, 427-432,
495 <https://doi.org/10.1021/acs.estlett.7b00352>, 2017.

496 Loza, C. L., Coggon, M. M., Nguyen, T. B., Zuend, A., Flagan, R. C. and Seinfeld, J.
497 H.: On the mixing and evaporation of secondary organic aerosol components,
498 *Environ. Sci. Technol.*, 47, 6173-6180, <https://doi.org/10.1021/es400979k>,
499 2013.

500 Maclean, A. M., Butenhoff, C. L., Grayson, J. W., Barsanti, K., Jimenez, J. L. and
501 Bertram, A. K.: Mixing times of organic molecules within secondary organic
502 aerosol particles: a global planetary boundary layer perspective, *Atmos. Chem.*
503 *Phys.*, 17, 13037-13048, <https://doi.org/10.5194/acp-17-13037-2017>, 2017.

504 Mai, H., Shiraiwa, M., Flagan, R. C. and Seinfeld, J. H.: Under what conditions can
505 equilibrium gas-particle partitioning be expected to hold in the atmosphere?,
506 *Environ. Sci. Technol.*, 49, 11485-11491,
507 <https://doi.org/10.1021/acs.est.5b02587>, 2015.

508 Maria, S. F., Russell, L. M., Gilles, M. K. and Myneni, S. C. B.: Organic aerosol
509 growth mechanisms and their climate-forcing implications, *Science*, 306,
510 1921-1924, <https://doi.org/10.1126/science.1103491>, 2004.

511 Marshall, F. H., Miles, R. E., Song, Y.-C., Ohm, P. B., Power, R. M., Reid, J. P. and
512 Dutcher, C. S.: Diffusion and reactivity in ultraviscous aerosol and the
513 correlation with particle viscosity, *Chem. Sci.*, 7, 1298-1308,
514 <https://doi.org/10.1039/C5SC03223G>, 2016.

515 Mu, Q., Shiraiwa, M., Octaviani, M., Ma, N., Ding, A., Su, H., Lammel, G., Pöschl,
516 U. and Cheng, Y.: Temperature effect on phase state and reactivity controls
517 atmospheric multiphase chemistry and transport of PAHs, *Sci. Adv.*, 4,
518 <https://doi.org/10.1126/sciadv.aap7314>, 2018.

519 O'Meara, S., Topping, D. O. and McFiggans, G.: The rate of equilibration of viscous
520 aerosol particles, *Atmos. Chem. Phys.*, 16, 5299-5313,
521 <https://doi.org/10.5194/acp-16-5299-2016>, 2016.

522 Pajunoja, A., Hu, W., Leong, Y. J., Taylor, N. F., Miettinen, P., Palm, B. B.,
523 Mikkonen, S., Collins, D. R., Jimenez, J. L. and Virtanen, A.: Phase state of
524 ambient aerosol linked with water uptake and chemical aging in the
525 southeastern US, *Atmos. Chem. Phys.*, 16, 11163-11176,
526 <https://doi.org/10.5194/acp-16-11163-2016>, 2016.

527 Pankow, J. F.: An absorption model of gas-particle partitioning of organic-compounds
528 in the atmosphere, *Atmos. Environ.*, 28, 185-188,
529 [https://doi.org/10.1016/1352-2310\(94\)90093-0](https://doi.org/10.1016/1352-2310(94)90093-0), 1994.

530 Perraud, V., Bruns, E. A., Ezell, M. J., Johnson, S. N., Yu, Y., Alexander, M. L.,
531 Zelenyuk, A., Imre, D., Chang, W. L., Dabdub, D., Pankow, J. F. and
532 Finlayson-Pitts, B. J.: Nonequilibrium atmospheric secondary organic aerosol
533 formation and growth, *Proc. Natl. Acad. Sci. U.S.A.*, 109, 2836-2841,
534 <https://doi.org/10.1073/pnas.1119909109>, 2012.

535 Petters, M. D. and Kreidenweis, S. M.: A single parameter representation of
536 hygroscopic growth and cloud condensation nucleus activity, *Atmos. Chem.*
537 *Phys.*, 7, 1961-1971, <https://doi.org/10.5194/acp-7-1961-2007>, 2007.

538 Petters, S. S., Kreidenweis, S. M., Grieshop, A. P., Ziemann, P. J. and Petters, M. D.:
539 Temperature- and humidity-dependent phase states of secondary organic
540 aerosols, *Geophys. Res. Lett.*, 46, <https://doi.org/10.1029/2018GL080563>,
541 2019.

542 Pfrang, C., Shiraiwa, M. and Pöschl, U.: Chemical ageing and transformation of
543 diffusivity in semi-solid multi-component organic aerosol particles, *Atmos.*
544 *Chem. Phys.*, 11, 7343-7354, <https://doi.org/10.5194/acp-11-7343-2011>, 2011.

545 Pöhlker, C., Wiedemann, K. T., Sinha, B., Shiraiwa, M., Gunthe, S. S., Smith, M., Su,
546 H., Artaxo, P., Chen, Q., Cheng, Y., Elbert, W., Gilles, M. K., Kilcoyne, A. L.
547 D., Moffet, R. C., Weigand, M., Martin, S. T., Pöschl, U. and Andreae, M. O.:
548 Biogenic potassium salt particles as seeds for secondary organic aerosol in the
549 Amazon, *Science*, 337, 1075-1078, <https://doi.org/10.1126/science.1223264>,
550 2012.

551 Price, H. C., Mattsson, J., Zhang, Y., Bertram, A. K., Davies, J. F., Grayson, J. W.,
552 Martin, S. T., O'Sullivan, D., Reid, J. P., Rickards, A. M. and Murray, B. J.:
553 Water diffusion in atmospherically relevant α -pinene secondary organic
554 material, *Chem. Sci.*, 6, 4876-4883, <https://doi.org/10.1039/c5sc00685f>, 2015.

555 Pye, H. O. T., Murphy, B. N., Xu, L., Ng, N. L., Carlton, A. G., Guo, H., Weber, R.,
556 Vasilakos, P., Appel, K. W., Budisulistiorini, S. H., Surratt, J. D., Nenes, A.,
557 Hu, W., Jimenez, J. L., Isaacman-VanWertz, G., Misztal, P. K. and Goldstein,
558 A. H.: On the implications of aerosol liquid water and phase separation for
559 organic aerosol mass, *Atmos. Chem. Phys.*, 17, 343-369,
560 <https://doi.org/10.5194/acp-17-343-2017>, 2017.

561 Reid, J. P., Bertram, A. K., Topping, D. O., Laskin, A., Martin, S. T., Petters, M. D.,
562 Pope, F. D. and Rovelli, G.: The viscosity of atmospherically relevant organic
563 particles, *Nat. Commun.*, 9, 956, <https://doi.org/10.1038/s41467-018-03027-z>,
564 2018.

565 Renbaum-Wolff, L., Song, M., Marcolli, C., Zhang, Y., Liu, P. F., Grayson, J. W.,
566 Geiger, F. M., Martin, S. T. and Bertram, A. K.: Observations and
567 implications of liquid-liquid phase separation at high relative humidities in
568 secondary organic material produced by α -pinene ozonolysis without
569 inorganic salts, *Atmos. Chem. Phys.*, 16, 7969-7979,
570 <https://doi.org/10.5194/acp-16-7969-2016>, 2016.

571 Riedel, T. P., Lin, Y. H., Zhang, Z., Chu, K., Thornton, J. A., Vizuete, W., Gold, A.
572 and Surratt, J. D.: Constraining condensed-phase formation kinetics of
573 secondary organic aerosol components from isoprene epoxydiols, *Atmos.*
574 *Chem. Phys.*, 16, 1245-1254, <https://doi.org/10.5194/acp-16-1245-2016>, 2016.

575 Riipinen, I., Pierce, J. R., Yli-Juuti, T., Nieminen, T., Hakkinen, S., Ehn, M.,
576 Junninen, H., Lehtipalo, K., Petaja, T., Slowik, J., Chang, R., Shantz, N. C.,
577 Abbatt, J., Leaitch, W. R., Kerminen, V. M., Worsnop, D. R., Pandis, S. N.,
578 Donahue, N. M. and Kulmala, M.: Organic condensation: a vital link
579 connecting aerosol formation to cloud condensation nuclei (CCN)
580 concentrations, *Atmos. Chem. Phys.*, 11, 3865-3878,
581 <https://doi.org/10.5194/acp-11-3865-2011>, 2011.

582 Riipinen, I., Yli-Juuti, T., Pierce, J. R., Petaja, T., Worsnop, D. R., Kulmala, M. and
583 Donahue, N. M.: The contribution of organics to atmospheric nanoparticle
584 growth, *Nat. Geosci.*, 5, 453-458, <https://doi.org/10.1038/ngeo1499>, 2012.

585 Roldin, P., Eriksson, A. C., Nordin, E. Z., Hermansson, E., Mogensen, D., Rusanen,
586 A., Boy, M., Swietlicki, E., Svenningsson, B., Zelenyuk, A. and Pagels, J.:
587 Modelling non-equilibrium secondary organic aerosol formation and
588 evaporation with the aerosol dynamics, gas- and particle-phase chemistry
589 kinetic multilayer model ADCHAM, *Atmos. Chem. Phys.*, 14, 7953-7993,
590 <https://doi.org/10.5194/acp-14-7953-2014>, 2014.

591 Rothfuss, N. E. and Petters, M. D.: Characterization of the temperature and
592 humidity-dependent phase diagram of amorphous nanoscale organic aerosols,
593 *Phys. Chem. Chem. Phys.*, 19, 6532-6545,
594 <https://doi.org/10.1039/C6CP08593H>, 2017.

595 Saha, P. K. and Grieshop, A. P.: Exploring divergent volatility properties from yield
596 and thermodynamic measurements of secondary organic aerosol from α -pinene
597 ozonolysis, *Environ. Sci. Technol.*, 50, 5740-5749,
598 <https://doi.org/10.1021/acs.est.6b00303>, 2016.

599 Saleh, R., Donahue, N. M. and Robinson, A. L.: Time scales for gas-particle
600 partitioning equilibration of secondary organic aerosol formed from
601 alpha-pinene ozonolysis, *Environ. Sci. Technol.*, 47, 5588-5594,
602 <https://doi.org/10.1021/es400078d>, 2013.

603 Seinfeld, J. H. and Pandis, S. N.: Atmospheric chemistry and physics - From air
604 pollution to climate change, John Wiley & Sons, Inc., New York, 2006.

605 Shiraiwa, M., Ammann, M., Koop, T. and Poschl, U.: Gas uptake and chemical aging
606 of semisolid organic aerosol particles, *Proc. Natl. Acad. Sci. U.S.A.*, 108,
607 11003-11008, <https://doi.org/10.1073/pnas.1103045108>, 2011.

608 Shiraiwa, M., Pfrang, C., Koop, T. and Pöschl, U.: Kinetic multi-layer model of
609 gas-particle interactions in aerosols and clouds (KM-GAP): linking
610 condensation, evaporation and chemical reactions of organics, oxidants and
611 water, *Atmos. Chem. Phys.*, 12, 2777-2794,
612 <https://doi.org/10.5194/acp-12-2777-2012>, 2012.

613 Shiraiwa, M. and Seinfeld, J. H.: Equilibration timescale of atmospheric secondary
614 organic aerosol partitioning, *Geophys. Res. Lett.*, 39, L24801,
615 <https://doi.org/10.1029/2012GL054008>, 2012.

616 Shiraiwa, M., Yee, L. D., Schilling, K. A., Loza, C. L., Craven, J. S., Zuend, A.,
617 Ziemann, P. J. and Seinfeld, J. H.: Size distribution dynamics reveal
618 particle-phase chemistry in organic aerosol formation, *Proc. Natl. Acad. Sci.*
619 *U.S.A.*, 110, 11746-11750, <https://doi.org/10.1073/pnas.1307501110>, 2013a.

620 Shiraiwa, M., Zuend, A., Bertram, A. K. and Seinfeld, J. H.: Gas-particle partitioning
621 of atmospheric aerosols: interplay of physical state, non-ideal mixing and
622 morphology, *Phys. Chem. Chem. Phys.*, 15, 11441-11453,
623 <https://doi.org/10.1039/C3CP51595H>, 2013b.

624 Shiraiwa, M., Li, Y., Tsimpidi, A. P., Karydis, V. A., Berkemeier, T., Pandis, S. N.,
625 Lelieveld, J., Koop, T. and Pöschl, U.: Global distribution of particle phase
626 state in atmospheric secondary organic aerosols, *Nat. Commun.*, 8, 15002,
627 <https://doi.org/10.1038/ncomms15002>, 2017.

628 Shrivastava, M., Cappa, C. D., Fan, J., Goldstein, A. H., Guenther, A. B., Jimenez, J.
629 L., Kuang, C., Laskin, A., Martin, S. T., Ng, N. L., Petaja, T., Pierce, J. R.,
630 Rasch, P. J., Roldin, P., Seinfeld, J. H., Shilling, J., Smith, J. N., Thornton, J.
631 A., Volkamer, R., Wang, J., Worsnop, D. R., Zaveri, R. A., Zelenyuk, A. and
632 Zhang, Q.: Recent advances in understanding secondary organic aerosol:
633 Implications for global climate forcing, *Rev. Geophys.*, 55, 509-559,
634 <https://doi.org/10.1002/2016RG000540>, 2017a.

635 Shrivastava, M., Lou, S., Zelenyuk, A., Easter, R. C., Corley, R. A., Thrall, B. D.,
636 Rasch, P. J., Fast, J. D., Simonich, S. L. M., Shen, H. and Tao, S.: Global
637 long-range transport and lung cancer risk from polycyclic aromatic
638 hydrocarbons shielded by coatings of organic aerosol, *Proc. Natl. Acad. Sci.*
639 *U.S.A.*, 114, 1246-1251, <https://doi.org/10.1073/pnas.1618475114>, 2017b.

640 Slade, J. H., Shiraiwa, M., Arangio, A., Su, H., Pöschl, U., Wang, J. and Knopf, D.
641 A.: Cloud droplet activation through oxidation of organic aerosol influenced
642 by temperature and particle phase state, *Geophys. Res. Lett.*, 41, 5297-5306,
643 <https://doi.org/10.1002/2014GL060582>, 2017.

644 Tong, H., Arangio, A. M., Lakey, P. S. J., Berkemeier, T., Liu, F., Kampf, C. J.,
645 Brune, W. H., Pöschl, U. and Shiraiwa, M.: Hydroxyl radicals from secondary
646 organic aerosol decomposition in water, *Atmos. Chem. Phys.*, 16, 1761-1771,
647 <https://doi.org/10.5194/acp-16-1761-2016>, 2016.

648 Tröstl, J., Chuang, W. K., Gordon, H., Heinritzi, M., Yan, C., Molteni, U., Ahlm, L.,
649 Frege, C., Bianchi, F., Wagner, R., Simon, M., Lehtipalo, K., Williamson, C.,
650 Craven, J. S., Duplissy, J., Adamov, A., Almeida, J., Bernhammer, A.-K.,
651 Breitenlechner, M., Brilke, S., Dias, A., Ehrhart, S., Flagan, R. C., Franchin,
652 A., Fuchs, C., Guida, R., Gysel, M., Hansel, A., Hoyle, C. R., Jokinen, T.,
653 Junninen, H., Kangasluoma, J., Keskinen, H., Kim, J., Krapf, M., Kürten, A.,
654 Laaksonen, A., Lawler, M., Leiminger, M., Mathot, S., Möhler, O., Nieminen,
655 T., Onnela, A., Petäjä, T., Piel, F. M., Miettinen, P., Rissanen, M. P., Rondo,
656 L., Sarnela, N., Schobesberger, S., Sengupta, K., Sipilä, M., Smith, J. N.,
657 Steiner, G., Tomè, A., Virtanen, A., Wagner, A. C., Weingartner, E., Wimmer,
658 D., Winkler, P. M., Ye, P., Carslaw, K. S., Curtius, J., Dommen, J., Kirkby, J.,
659 Kulmala, M., Riipinen, I., Worsnop, D. R., Donahue, N. M. and
660 Baltensperger, U.: The role of low-volatility organic compounds in initial
661 particle growth in the atmosphere, *Nature*, 533, 527-531,
662 <https://doi.org/10.1038/nature18271>, 2016.

663 Vaden, T. D., Imre, D., Beránek, J., Shrivastava, M. and Zelenyuk, A.: Evaporation
664 kinetics and phase of laboratory and ambient secondary organic aerosol, *Proc.*
665 *Natl. Acad. Sci. U.S.A.*, 108, 2190-2195,
666 <https://doi.org/10.1073/pnas.1013391108>, 2011.

667 Virtanen, A., Joutsensaari, J., Koop, T., Kannosto, J., Yli-Pirilä, P., Leskinen, J.,
668 Mäkelä, J. M., Holopainen, J. K., Pöschl, U. and Kulmala, M.: An amorphous
669 solid state of biogenic secondary organic aerosol particles, *Nature*, 467,
670 824-827, <https://doi.org/10.1038/nature09455>, 2010.

671 Wang, J., Krejci, R., Giangrande, S., Kuang, C., Barbosa, H. M. J., Brito, J., Carbone,
672 S., Chi, X., Comstock, J., Ditas, F., Lavric, J., Manninen, H. E., Mei, F.,
673 Moran-Zuloaga, D., Pöhlker, C., Pöhlker, M. L., Saturno, J., Schmid, B.,
674 Souza, R. A. F., Springston, S. R., Tomlinson, J. M., Toto, T., Walter, D.,
675 Wimmer, D., Smith, J. N., Kulmala, M., Machado, L. A. T., Artaxo, P.,
676 Andreae, M. O., Petäjä, T. and Martin, S. T.: Amazon boundary layer aerosol
677 concentration sustained by vertical transport during rainfall, *Nature*, 539,
678 416-419, <https://doi.org/10.1038/nature19819>, 2016.

679 Ye, J., Gordon, C. A. and Chan, A. W. H.: Enhancement in secondary organic aerosol
680 formation in the presence of preexisting organic particle, *Environ. Sci.*
681 *Technol.*, 50, 3572-3579, <https://doi.org/10.1021/acs.est.5b05512>, 2016a.

682 Ye, Q., Robinson, E. S., Ding, X., Ye, P., Sullivan, R. C. and Donahue, N. M.:
683 Mixing of secondary organic aerosols versus relative humidity, *Proc. Natl.*
684 *Acad. Sci. U.S.A.*, 113, 12649-12654,
685 <https://doi.org/10.1073/pnas.1604536113>, 2016b.

686 Ye, Q., Upshur, M. A., Robinson, E. S., Geiger, F. M., Sullivan, R. C., Thomson, R.
687 J. and Donahue, N. M.: Following particle-particle mixing in atmospheric
688 secondary organic aerosols by using isotopically labeled terpenes, *Chem*, 4,
689 318-333, <https://doi.org/10.1016/j.chempr.2017.12.008>, 2018.

690 Yli-Juuti, T., Pajunoja, A., Tikkanen, O.-P., Buchholz, A., Faiola, C., Väisänen, O.,
691 Hao, L., Kari, E., Peräkylä, O., Garmash, O., Shiraiwa, M., Ehn, M., Lehtinen,
692 K. and Virtanen, A.: Factors controlling the evaporation of secondary organic
693 aerosol from α -pinene ozonolysis, *Geophys. Res. Lett.*, 44, 2562-2570,
694 <https://doi.org/10.1002/2016GL072364>, 2017.

695 You, Y., Renbaum-Wolff, L., Carreras-Sospedra, M., Hanna, S. J., Hiranuma, N.,
696 Kamal, S., Smith, M. L., Zhang, X., Weber, R. J., Shilling, J. E., Dabdub, D.,
697 Martin, S. T. and Bertram, A. K.: Images reveal that atmospheric particles can
698 undergo liquid-liquid phase separations, *Proc. Natl. Acad. Sci. U.S.A.*, 109,
699 13188-13193, <https://doi.org/10.1073/pnas.1206414109>, 2012.

700 You, Y., Smith, M. L., Song, M., Martin, S. T. and Bertram, A. K.: Liquid-liquid
701 phase separation in atmospherically relevant particles consisting of organic
702 species and inorganic salts, *Int. Rev. Phys. Chem.*, 33, 43-77,
703 <https://doi.org/10.1080/0144235X.2014.890786>, 2014.

704 Zaveri, R. A., Easter, R. C., Shilling, J. E. and Seinfeld, J. H.: Modeling kinetic
705 partitioning of secondary organic aerosol and size distribution dynamics:
706 representing effects of volatility, phase state, and particle-phase reaction,
707 *Atmos. Chem. Phys.*, 14, 5153-5181,
708 <https://doi.org/10.5194/acp-14-5153-2014>, 2014.

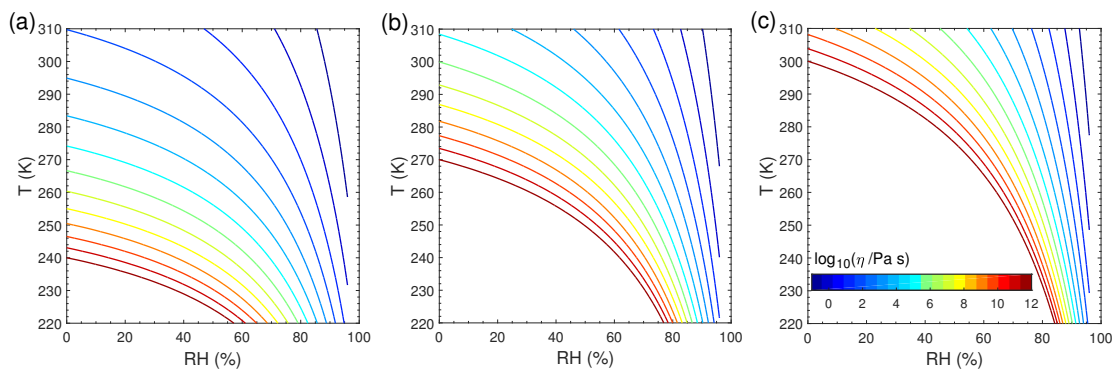
709 Zaveri, R. A., Shilling, J. E., Zelenyuk, A., Liu, J., Bell, D. M., D'Ambro, E. L.,
710 Gaston, C. J., Thornton, J. A., Laskin, A., Lin, P., Wilson, J., Easter, R. C.,
711 Wang, J., Bertram, A. K., Martin, S. T., Seinfeld, J. H. and Worsnop, D. R.:
712 Growth kinetics and size distribution dynamics of viscous secondary organic
713 aerosol, *Environ. Sci. Technol.*, 52, 1191-1199,
714 <https://doi.org/10.1021/acs.est.7b04623>, 2018.

715 Zhang, X., Pandis, S. N. and Seinfeld, J. H.: Diffusion-limited versus
716 quasi-equilibrium aerosol growth, *Aerosol Sci. Technol.*, 46, 874-885,
717 <https://doi.org/10.1080/02786826.2012.679344>, 2012.

718 Zhang, Y., Sanchez, M. S., Douet, C., Wang, Y., Bateman, A. P., Gong, Z., Kuwata,
719 M., Renbaum-Wolff, L., Sato, B. B., Liu, P. F., Bertram, A. K., Geiger, F. M.
720 and Martin, S. T.: Changing shapes and implied viscosities of suspended
721 submicron particles, *Atmos. Chem. Phys.*, 15, 7819-7829,
722 <https://doi.org/10.5194/acp-15-7819-2015>, 2015.

723 Zhang, Y., Chen, Y., Lambe, A. T., Olson, N. E., Lei, Z., Craig, R. L., Zhang, Z.,
724 Gold, A., Onasch, T. B., Jayne, J. T., Worsnop, D. R., Gaston, C. J., Thornton,
725 J. A., Vizuite, W., Ault, A. P. and Surratt, J. D.: Effect of the Aerosol-Phase
726 State on Secondary Organic Aerosol Formation from the Reactive Uptake of
727 Isoprene-Derived Epoxydiols (IEPOX), *Environ. Sci. Technol. Lett.*,
728 <https://doi.org/10.1021/acs.estlett.8b00044>, 2018.

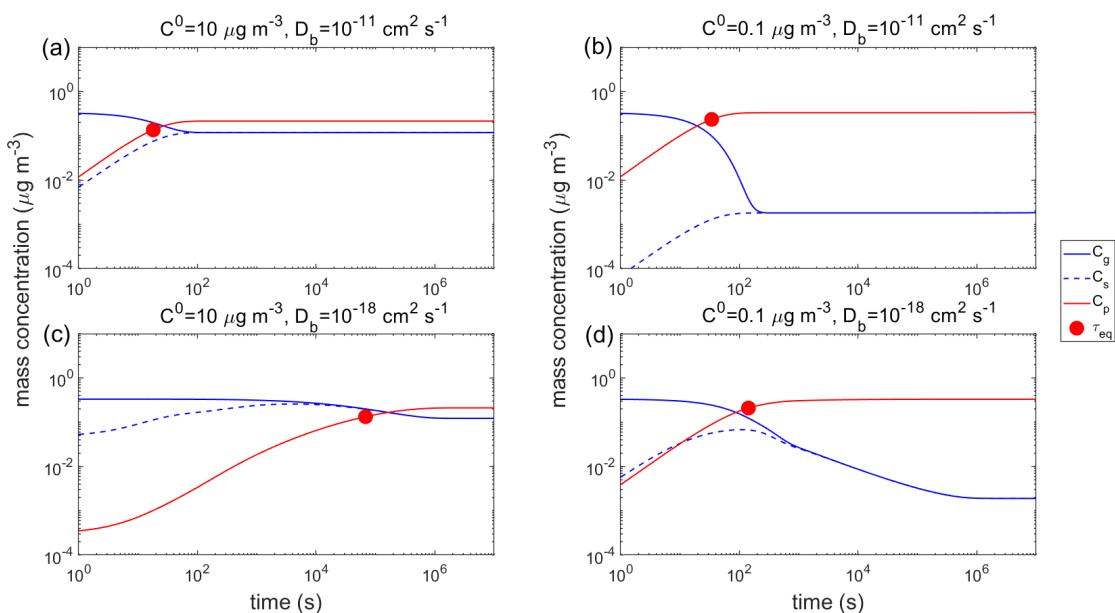
729



730

731 **Figure 1.** Viscosity of pre-existing particles as a function of temperature and relative
 732 humidity. The glass transition temperatures under dry conditions ($T_{g,org}$) are (a) 240 K,
 733 (b) 270 K, and (c) 300 K, respectively.

734

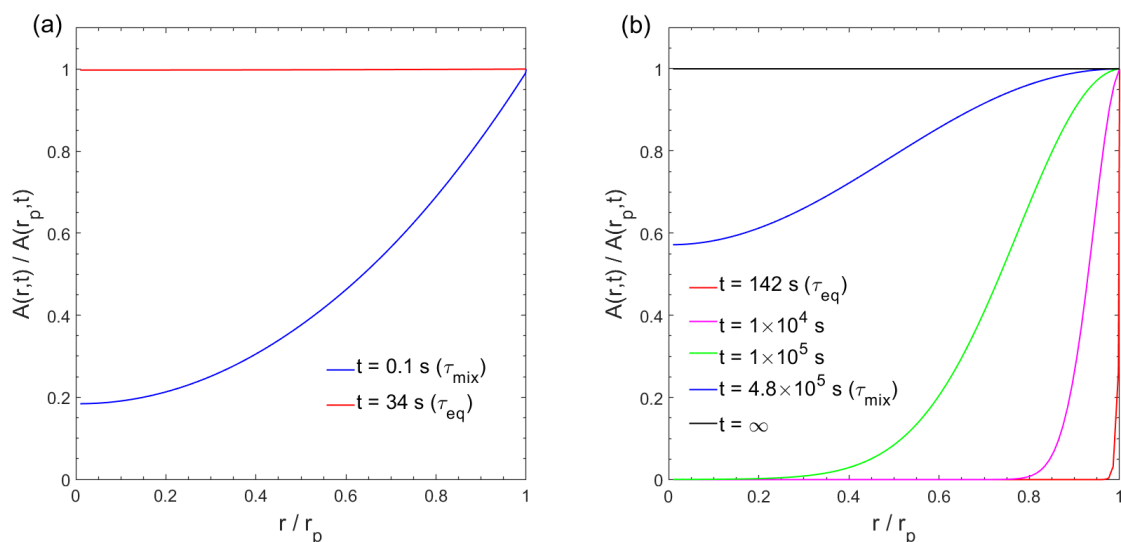


735

736 **Figure 2.** Temporal evolution of mass concentrations of the condensing compound Z
 737 in the gas phase (C_g), just above the particle surface (C_s), and in the particle phase
 738 (C_p) in the closed system. τ_{eq} is marked with the red circle. RH = 60% and T is (a–b)
 739 298 K and (c–d) 250 K. The C^0 of Z is (a, c) $10 \mu\text{g m}^{-3}$ and (b, d) $0.1 \mu\text{g m}^{-3}$. The
 740 glass transition temperature of pre-existing particles under dry conditions ($T_{g,org}$) is set
 741 to be 270 K, which leads to D_b of (a–b) $10^{-11} \text{ cm}^2 \text{ s}^{-1}$ and (c–d) $10^{-18} \text{ cm}^2 \text{ s}^{-1}$. The
 742 initial mass concentration of pre-existing particles is set to be $20 \mu\text{g m}^{-3}$ with the
 743 number concentrations of $3 \times 10^4 \text{ cm}^{-3}$ and the initial particle diameter of 100 nm.

744

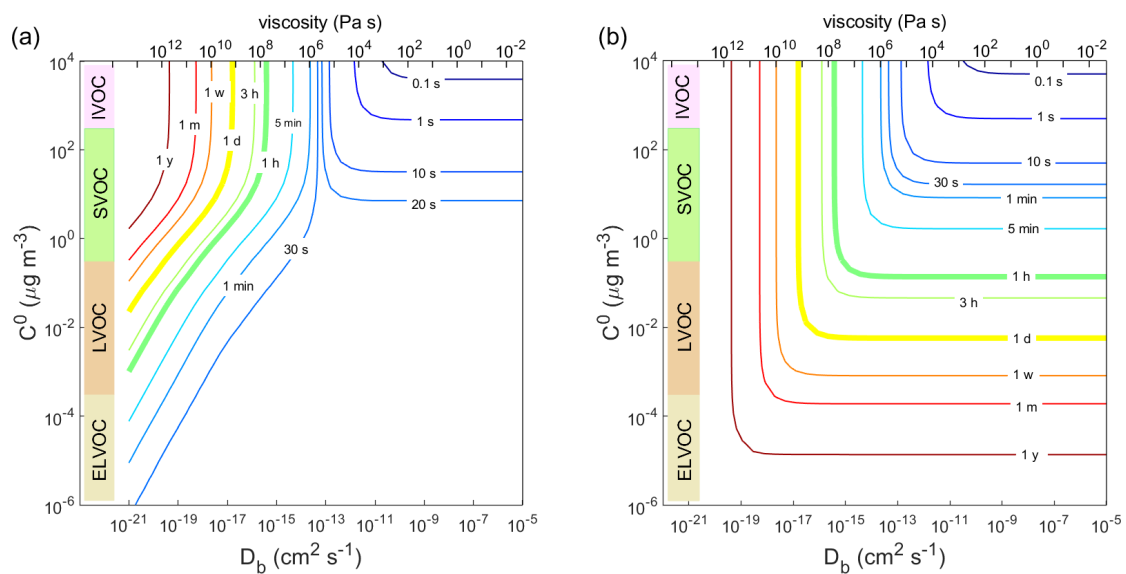
745



746

747 **Figure 3.** Dimensionless radial concentration profiles in the particle for the
 748 condensation of the LVOC species ($C^0 = 0.1 \mu\text{g m}^{-3}$) at RH = 60% and (a) $T = 298 \text{ K}$
 749 with $D_b = 10^{-11} \text{ cm}^2 \text{ s}^{-1}$ and (b) $T = 250 \text{ K}$ with $D_b = 10^{-18} \text{ cm}^2 \text{ s}^{-1}$. The x-axis indicates
 750 the radial distance from the particle center (r) normalized by the particle radius (r_p),
 751 ranging from the particle core ($r / r_p \approx 0$) to the surface ($r / r_p = 1$). The y-axis indicates
 752 the bulk concentration of the condensing compound at a given position in the bulk (r)
 753 normalized by the bulk concentration at particle surface (r_p).

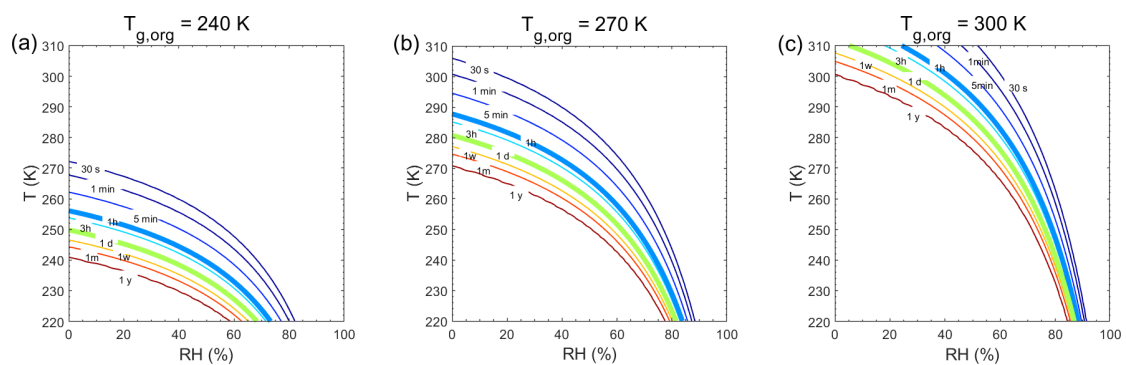
754



755

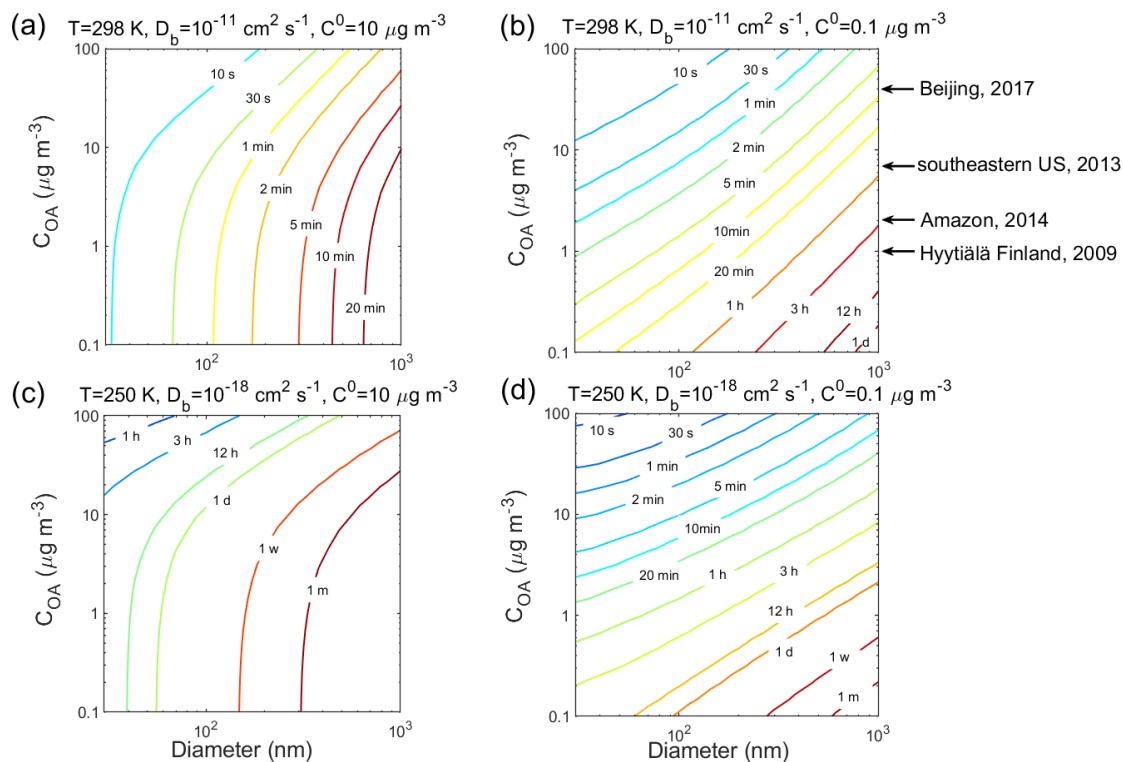
756 **Figure 4.** Contour plot of equilibration timescale (τ_{eq}) as a function of bulk diffusivity
 757 (D_b) and saturation mass concentration (C^0) for (a) condensation in the closed system
 758 and (b) evaporation in the open system. The initial mass concentration of pre-existing
 759 particles is set to be $20 \mu\text{g m}^{-3}$ with the number concentrations of $3 \times 10^4 \text{ cm}^{-3}$ and the
 760 initial particle diameter of 100 nm. Viscosity is calculated from the Stokes-Einstein
 761 equation assuming the effective molecular radius of 10^{-8} cm at T of 298 K.

762



763

764 **Figure 5.** Equilibration timescale (τ_{eq}) as a function of temperature and relative
 765 humidity in the closed system. The glass transition temperatures of pre-existing
 766 particles at dry conditions ($T_{g,org}$) are (a) 240 K, (b) 270 K, and (c) 300 K,
 767 respectively. The saturation mass concentration (C^0) of the condensing compound is
 768 $10 \mu\text{g m}^{-3}$ (SVOC). The mass concentration of pre-existing particles is set to be $20 \mu\text{g}$
 769 m^{-3} with the number concentrations of $3 \times 10^4 \text{ cm}^{-3}$ and the initial particle diameter of
 770 100 nm.

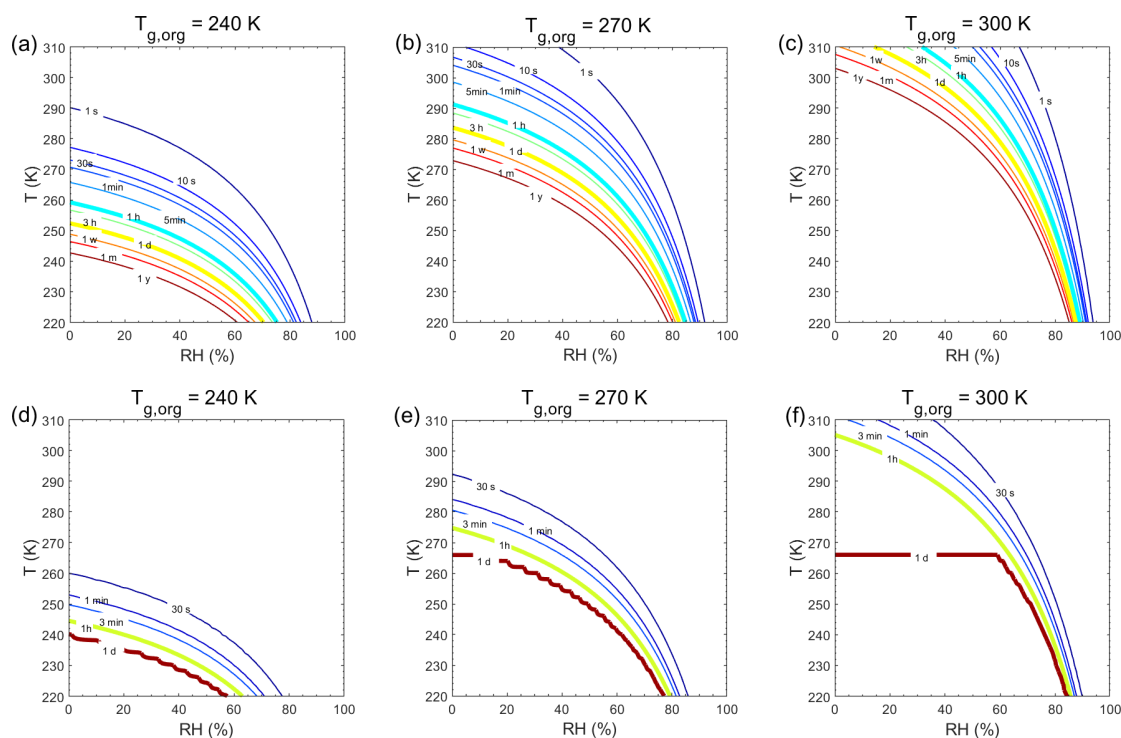


771

772 **Figure 6.** Equilibration timescale (τ_{eq}) for (a, c) SVOC ($C^0 = 10 \mu\text{g m}^{-3}$) and (b, d)
 773 LVOC ($C^0 = 0.1 \mu\text{g m}^{-3}$) as a function of particle diameter (nm) and mass
 774 concentration ($\mu\text{g m}^{-3}$) of pre-existing particles at 60% RH and T of (a-b) 298 K and
 775 (c-d) 250 K in the closed system. The glass transition temperature of pre-existing
 776 particles under dry conditions ($T_{g,org}$) is set to be 270 K, which leads to D_b of (a-b)
 777 $10^{-11} \text{ cm}^2 \text{ s}^{-1}$ and (c-d) $10^{-18} \text{ cm}^2 \text{ s}^{-1}$. Ambient organic mass concentrations are
 778 indicated with arrows.

779

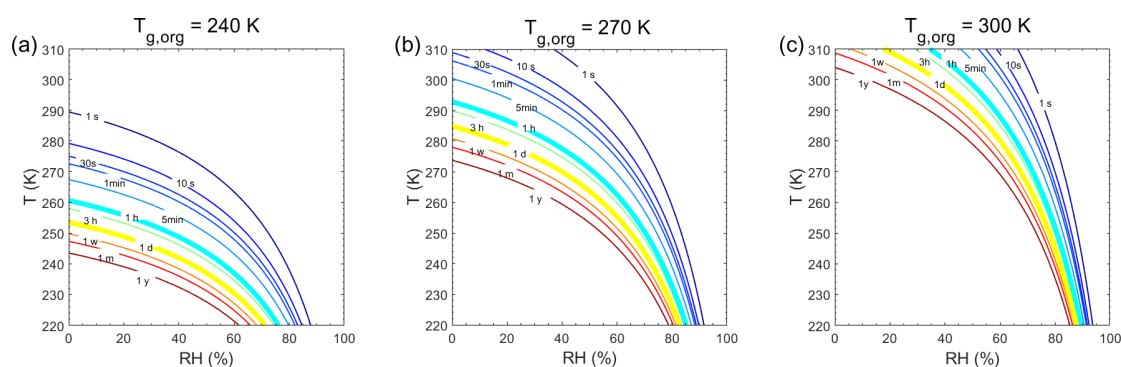
780 **Appendix:**



781

782

783 **Figure A1.** Equilibration timescale (τ_{eq}) as a function of temperature and relative
 784 humidity in the closed system. The glass transition temperatures of pre-existing
 785 particles at dry conditions ($T_{g,org}$) are set to be (a, d) 240 K, (b, e) 270 K, and (c, f) 300
 786 K. The mass concentration of pre-existing particles is $20 \mu\text{g m}^{-3}$. The saturation mass
 787 concentration (C^0) of the condensing compound is (a, b, c) $10^3 \mu\text{g m}^{-3}$ and (d, e, f) 0.1
 788 $\mu\text{g m}^{-3}$.



789

790 **Figure A2.** Characteristic timescale of bulk diffusion or mixing timescale (τ_{mix}) as a
 791 function of temperature and relative humidity. The particle diameter is assumed to be
 792 100 nm with the glass transition temperatures of pre-existing particles at dry
 793 conditions ($T_{g,org}$) of (a) 240 K, (b), 270 K and (c) 300 K.

794

Supplement of

**Timescales of Secondary Organic Aerosols to Reach Equilibrium at
Various Temperatures and Relative Humidities**

Ying Li¹, and Manabu Shiraiwa^{1,*}

[1] Department of Chemistry, University of California, Irvine, California, USA.

*Correspondence to: Manabu Shiraiwa (m.shiraiwa@uci.edu)

Contents of this file

Tables S1 to S2

Figures S1 to S7

Table S1. Temperature-dependent kinetic parameters used in the simulations.

Parameter (Unit)	Description	Equation ^a
ω (cm s ⁻¹)	mean thermal velocity	$\omega(T) = (8RT/(\pi M))^{1/2}$
D_g (cm ² s ⁻¹)	gas-phase diffusion coefficient	$D_g(T, P) = (T/T_{\text{standard}})^{1.75} (P_{\text{standard}}/P) D_g(T_{\text{standard}}, P_{\text{standard}})^b$
D_b (cm ² s ⁻¹)	bulk diffusion coefficient	$D_b(T, RH) = kT/(6\pi a\eta(T, RH))$
k_a (cm s ⁻¹)	first-order adsorption rate coefficient	$k_a(T) = \alpha_s \omega(T)/4$
k_d (s ⁻¹)	first-order desorption rate coefficient	$k_d(T) = Ae^{-(E_{des}/(RT))}$
$k_{ss,s}$ (cm s ⁻¹)	first-order rate coefficient for quasi-static-to-sorption layer transport	$k_{ss,s}(T, RH) = 2D_b(T, RH) / (\delta_{ss} + \delta_z)$
$k_{s,ss}$ (s ⁻¹)	first-order rate coefficient for sorption-to-quasi-static surface transport	$k_{s,ss}(T, RH) = k_{ss,s}(T, RH)k_d(T)[Z]_{ss,eq} / (k_a(T)[Z]_{g,eq})$
$k_{b1,ss}$ (cm s ⁻¹)	rate coefficient of bulk layer 1-to-quasi-static surface transport	$k_{b1,ss}(T, RH) = 2D_b(T, RH) / (\delta_{ss} + \delta(1))$
$k_{ss,b1}$ (cm s ⁻¹)	rate coefficient of surface-to-bulk layer 1 transport	$k_{ss,b1}(T, RH) = k_{b1,ss}(T, RH)$
$k_{b,b}$ (cm s ⁻¹)	rate coefficient of transport between bulk layers	$k_{b,b}(T, RH) = 2D_b(T, RH) / (\delta(k) + \delta(k + 1))$
τ_d (s)	desorption lifetime	$\tau_d = k_d^{-1}$

^a Description and the values of the symbols shown in the equations are summarized in Table S2.

^b $D_g(T_{\text{standard}}, P_{\text{standard}})$ is calculated by the EPA on-line tools:

(<https://www3.epa.gov/ceampubl/learn2model/part-two/onsite/estdiffusion-ext.html>).

Table S2. Description and the values of the symbols in the equations of Table S1.

Variable (Unit)	Description	Value
R ($\text{J K}^{-1} \text{mol}^{-1}$)	gas constant	8.314
T (K)	temperature	varied from 220 to 310
RH (%)	relative humidity	varied from 0 to 100
M (g mol^{-1})	molar mass of compound Z	200
T_0 (K)	room temperature	298
ρ (g cm^{-3})	density of organic particles	1.4
P (Pa)	atmospheric pressure	$P = P_{\text{standard}} \times (T/T_{\text{standard}})^{g/LR}$
g (m s^{-2})	gravitational acceleration	9.8
R ($\text{m}^2 \text{s}^{-2} \text{K}^{-1}$)	gas constant of air	287
L (K m^{-1})	lapse rate	0.0065
T_{standard} (K)	sea level standard temperature in the International Standard Atmosphere	288.15
P_{standard} (Pa)	sea level standard atmospheric pressure in the International Standard Atmosphere	101325
K (J K^{-1})	Boltzmann constant	1.38×10^{-23}
a (cm)	effective molecular radius	10^{-8}
δ_Z (cm)	effective molecular diameter	2×10^{-8}
$\alpha_{s,0}$	surface accommodation coefficient on free-substrate	1
A (s^{-1})	pre-exponential factor	10^{12}
E_{des} (kJ mol^{-1})	desorption energy	40
$[Z]_{\text{g,eq}}$ (cm^{-3})	equilibrium (saturation) number concentrations of Z in the gas phase	variable
$[Z]_{\text{ss,eq}}$ (cm^{-2})	equilibrium (saturation) number concentrations of Z in the quasi-static surface layer	variable
δ_{ss} (cm)	thickness of the quasi-static surface layer	variable
$\delta(k)$ (cm)	thickness of the bulk layer k	variable

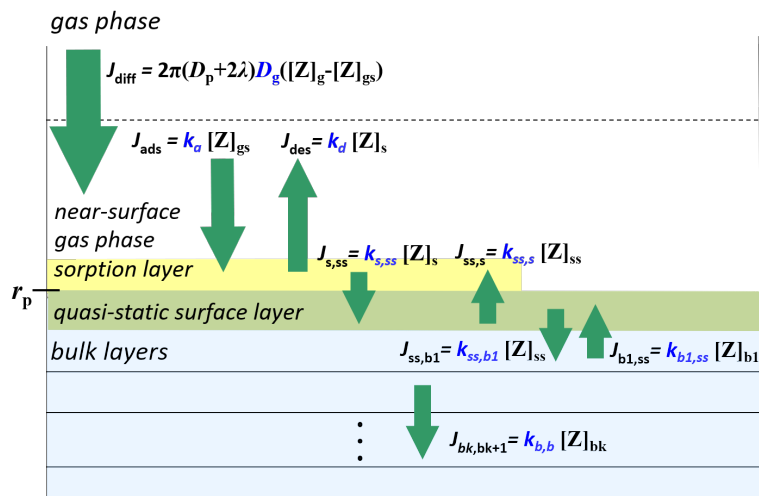


Figure S1. Temperature-dependent kinetic processes simulated in the KM-GAP model. Parameters in blue are treated as a function of temperature (Table S1). $[Z]$ are concentrations of species Z in the gas (g) and near-surface gas phases (gs), at the sorption layer (s) and in the surface (ss) and in the bulk (b) layers. J are the transport fluxes between each layer, including the gas-phase diffusion flux (J_{diff}), the adsorption (J_{ads}) and desorption (J_{des}) fluxes, surface–bulk exchange fluxes ($J_{s,ss}$, $J_{ss,s}$, $J_{ss,b1}$, $J_{b1,ss}$), and bulk diffusion fluxes ($J_{b,b}$).

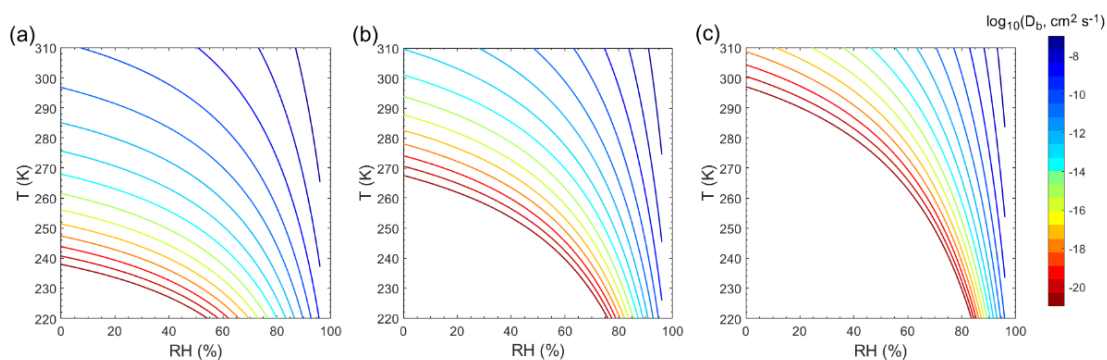


Figure S2. Bulk diffusion coefficient (D_b) in pre-existing particles as a function of temperature and relative humidity. The glass transition temperatures under dry conditions ($T_{g,\text{org}}$) are set to be (a) 240 K, (b) 270 K and (c) 300 K, respectively.

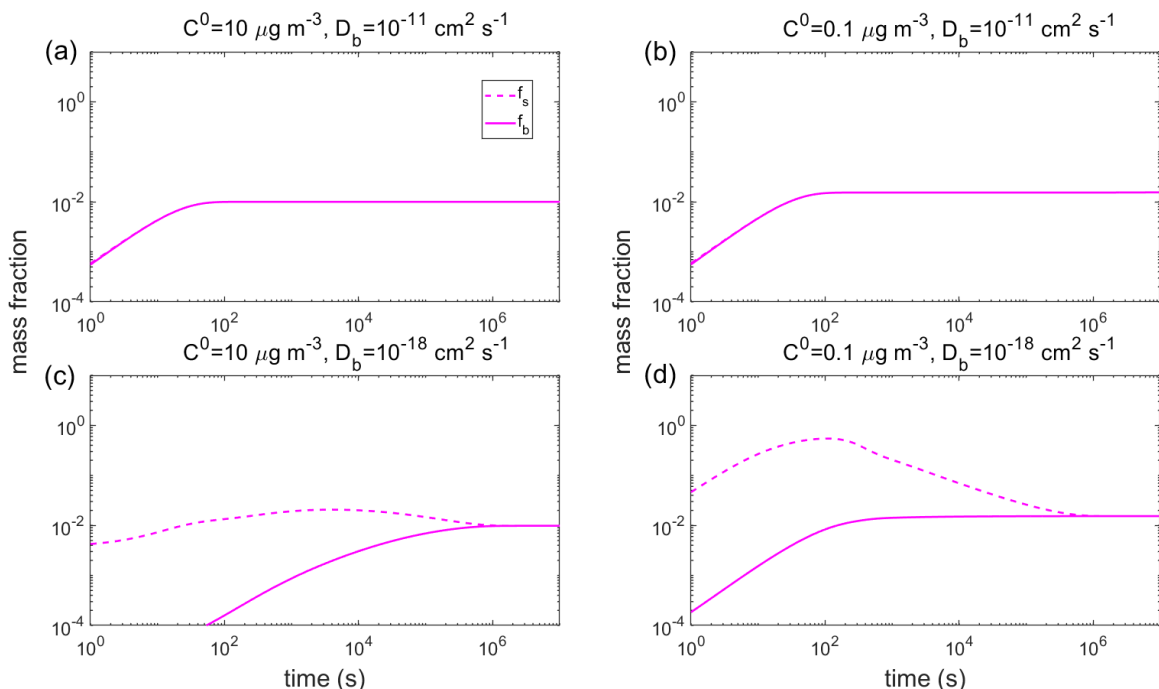


Figure S3. Temporal evolution of the mass fraction of Z in the near-surface bulk (f_s), and the average fraction of Z in the entire bulk (f_b). RH = 60% and T is (a, b) 298 K and (c, d) 250 K in the closed system. The C^0 of Z is (a, c) $10 \mu\text{g m}^{-3}$ and (b, d) $0.1 \mu\text{g m}^{-3}$. The glass transition temperature of pre-existing particles under dry conditions ($T_{g,\text{org}}$) is set to be 270 K, which leads to D_b of (a, b) $10^{-11} \text{cm}^2 \text{s}^{-1}$ and (c, d) $10^{-18} \text{cm}^2 \text{s}^{-1}$. The initial mass concentration of pre-existing particles is assumed to be $20 \mu\text{g m}^{-3}$ with the number concentrations of $3 \times 10^4 \text{cm}^{-3}$ and the initial particle diameter of 100 nm.

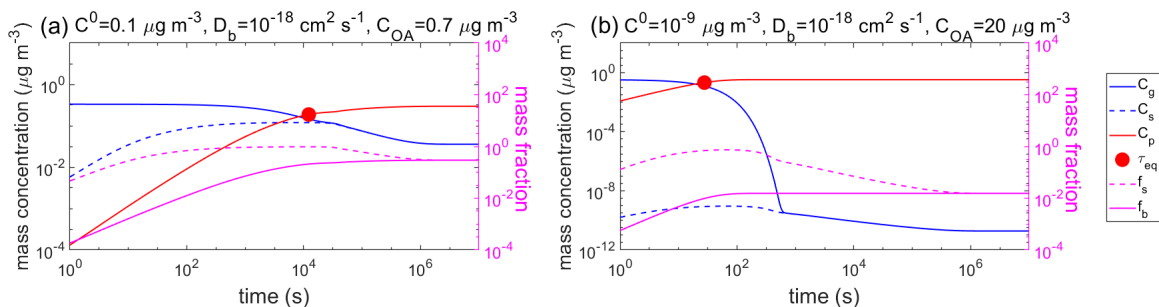


Figure S4. Temporal evolution of mass concentrations of the condensing compound Z in the gas phase (C_g), just above the particle surface (C_s), and in the particle phase (C_p) in the closed system. The mass fraction of Z in the near-surface bulk (f_s), and the average fraction of Z in the entire particle bulk (f_b) are also shown. D_b is $10^{-18} \text{cm}^2 \text{s}^{-1}$. The C^0 of Z is (a) $0.1 \mu\text{g m}^{-3}$ and (b) $10^{-9} \mu\text{g m}^{-3}$. The initial mass concentration of pre-existing particles is set to be (a) $0.7 \mu\text{g m}^{-3}$ and (b) $20 \mu\text{g m}^{-3}$.

$\mu\text{g m}^{-3}$. τ_{eq} is marked with the red circle. τ_{eq} (~ 28 s) in (b) is consistent with the inverse of the condensation sink (29 s).

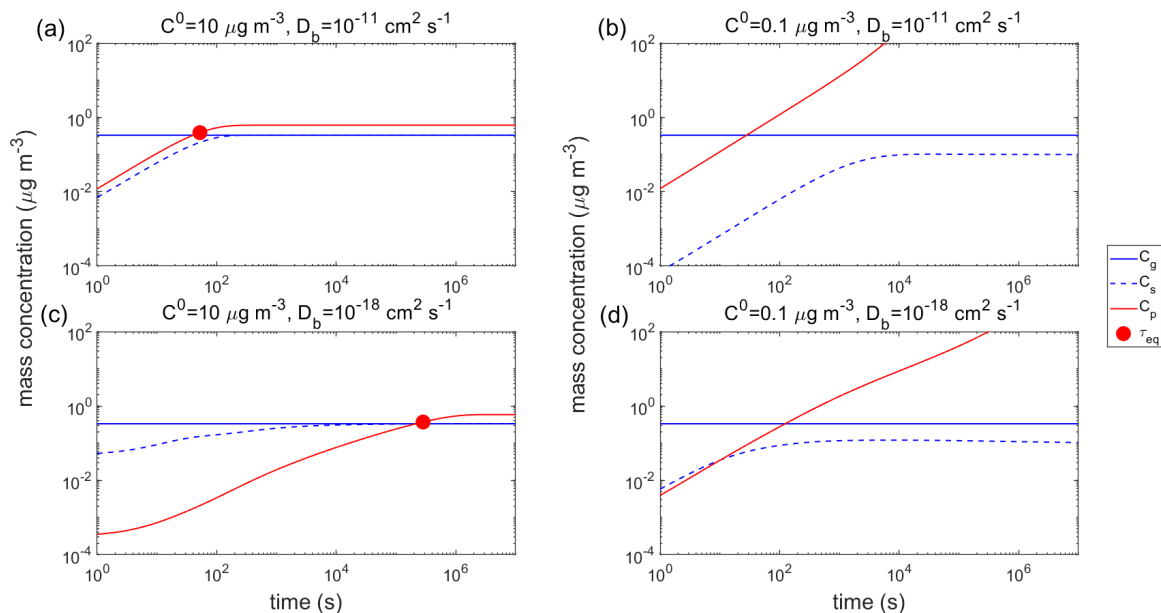


Figure S5. Temporal evolution of mass concentrations of the condensing compound Z in the gas phase (C_g), just above the particle surface (C_s), and in the particle phase (C_p) in the open system. τ_{eq} is marked with the red circle. RH = 60% and T is (a–b) 298 K and (c–d) 250 K. The C^0 of Z is (a, c) $10 \mu\text{g m}^{-3}$ and (b, d) $0.1 \mu\text{g m}^{-3}$. The glass transition temperature of pre-existing particles under dry conditions ($T_{\text{g,org}}$) is set to be 270 K, which leads to D_b of (a–b) $10^{-11} \text{ cm}^2 \text{ s}^{-1}$ and (c–d) $10^{-18} \text{ cm}^2 \text{ s}^{-1}$. The initial mass concentration of pre-existing particles is set to be $20 \mu\text{g m}^{-3}$ with the number concentrations of $3 \times 10^4 \text{ cm}^{-3}$ and the initial particle diameter of 100 nm.

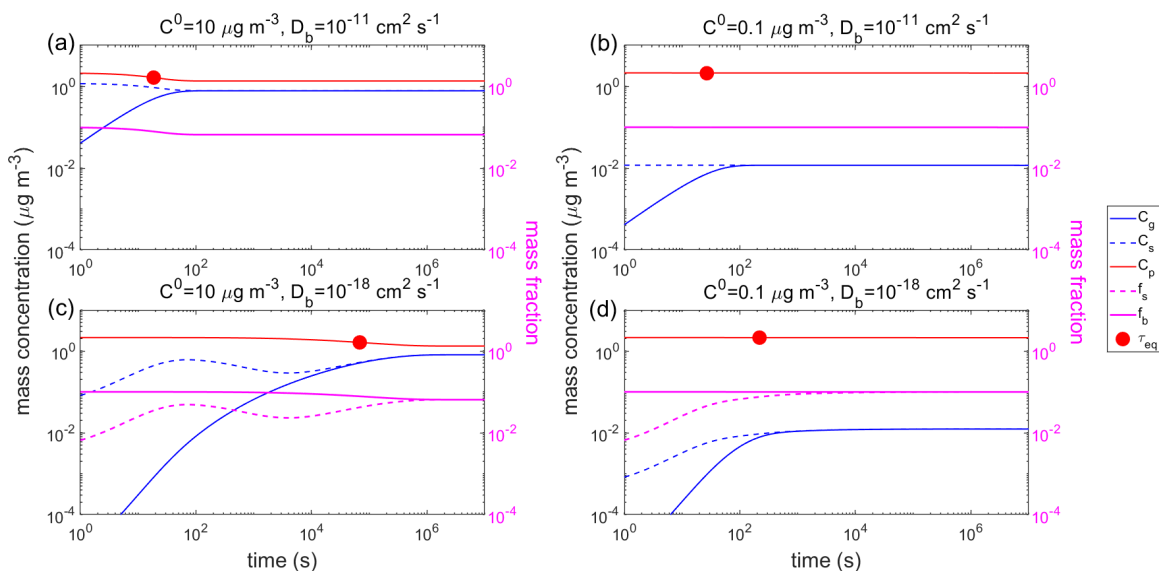


Figure S6. Temporal evolution of mass concentrations of the **evaporation** compound Z in the gas phase (C_g), just above particle surface (C_s), in the particle phase (C_p), the mass fraction of Z in the near-surface bulk (f_s), and the average fraction of Z in the entire particle bulk (f_b) **in the closed system**. τ_{eq} are marked with red circles. RH = 60% and T is (a–b) 298 K and (c–d) 250 K. The C^0 of the **evaporation** compound is (a, c) $10 \mu\text{g m}^{-3}$ and (b, d) $0.1 \mu\text{g m}^{-3}$. The glass transition temperature of pre-existing particles under dry conditions ($T_{g,org}$) is set to be 270 K, which leads to D_b of (a, b) $10^{-11} \text{cm}^2 \text{s}^{-1}$ and (c, d) $10^{-18} \text{cm}^2 \text{s}^{-1}$. The initial mass concentration of pre-existing non-volatile particles (C_{OA}) is assumed to be $20 \mu\text{g m}^{-3}$ with the number concentrations of $3 \times 10^4 \text{cm}^{-3}$ and the initial particle diameter of 100 nm.

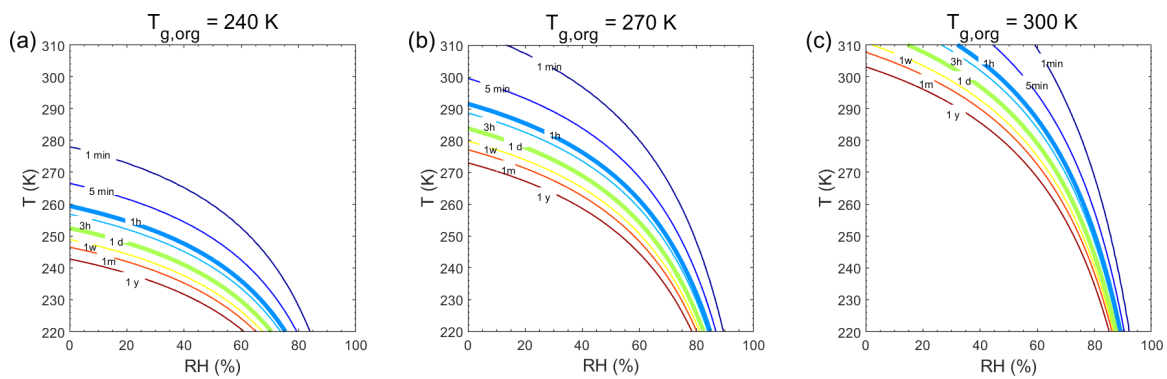


Figure S7. Equilibration timescale (τ_{eq}) as a function of temperature and relative humidity in the open system. The glass transition temperatures of pre-existing particles at dry conditions ($T_{g,org}$) are (a) 240 K, (b) 270 K, and (c) 300 K, respectively. The saturation mass concentration (C^0) of the condensing compound is $10 \mu\text{g m}^{-3}$ (SVOC). The mass concentration of pre-existing particles is set to be $20 \mu\text{g m}^{-3}$ with the number concentrations of $3 \times 10^4 \text{ cm}^{-3}$ and the initial particle diameter of 100 nm.